CHALMERS
UNIVERSITY OF TECHNOLOGY

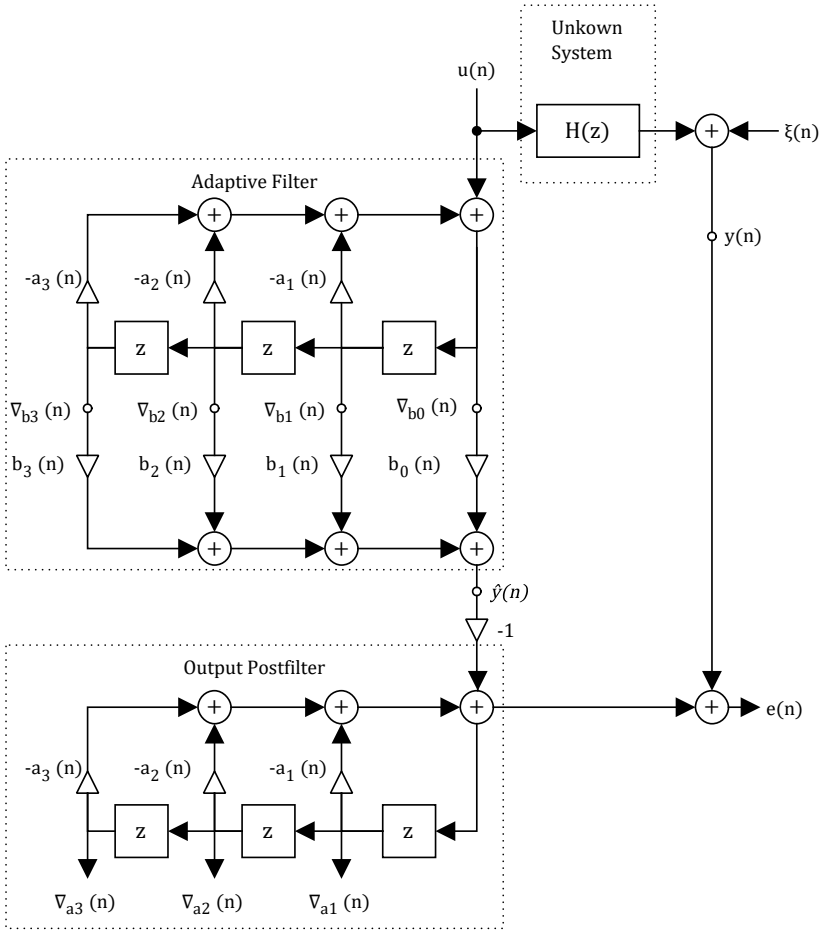

Gradient Descent Based Adaptive IIR Filtering with Direct and Lattice Form Filter Structures

Applied to Estimation of a Headphone Compensation Filter and Binaural Head Related Transfer Functions

Master's thesis in Sound and Vibration

ALEXANDER LENDON
DIVISION OF APPLIED ACOUSTICS
CHALMERS UNIVERSITY OF TECHNOLOGY
Gothenburg, Sweden 2025
www.chalmers.se

Master's thesis 2025

Gradient Descent Based Adaptive IIR Filtering with Direct and Lattice Form Filter Structures

Applied to Estimation of a Headphone Compensation Filter and Binaural Head Related Transfer Functions

ALEXANDER LENDON

CHALMERS
UNIVERSITY OF TECHNOLOGY

Department of Architecture and Civil Engineering
Division of Applied Acoustics
Chalmers University of Technology
Gothenburg, Sweden 2025

Gradient Descent Based Adaptive IIR Filtering with Direct and Lattice Form Filter Structures
Applied to estimation of a Headphone Compensation Filter and Binaural Head Related Transfer Functions
ALEXANDER LENDON

Supervisor: Jens Ahrens, Division of Applied Acoustics
Examiner: Jens Ahrens, Division of Applied Acoustics

Master's Thesis 2025
Department of Architecture and Civil Engineering
Division of Applied Acoustics
Chalmers University of Technology
SE-412 96 Gothenburg
Telephone +46 31-772 2200

Cover: A block flow diagram of an IIR adaptive filter in Direct Form.

Typeset in LaTeX
Printed by Chalmers Reproservice
Gothenburg, Sweden 2025

Gradient Descent Based Adaptive IIR Filtering with Direct and Lattice Form Filter Structures
Applied to estimation of a Headphone Compensation Filter and Binaural Head Related Transfer Functions
Alexander Lendon
Division of Applied Acoustics
Department of Architecture and Civil Engineering
Chalmers University of Technology

Abstract

In acoustic Digital Signal Processing (DSP), Finite Impulse Response (FIR) filters are commonly used due to their stability and ease of design. However, Infinite Impulse Response (IIR) filters offer better frequency resolution at lower filter orders, making them ideal for hardware-constrained applications like portable AR/VR headsets. With advances in computational methods, optimising IIR filters has become straightforward, making it important to compare their performance against traditional FIR filters.
This thesis investigates adaptive IIR filtering algorithms using Gradient Descent (GD) methods, applied to both direct form and lattice form filter structures. Lattice form filter structures provide the benefit of an in-built stability test which can guarantee that the produced IIR filter remains stable at each step. This is essential for reliable IIR filter design and allows for further modifications to the optimisation routine.
For the studies, the Modified GD direct form and the Simplified Partial Gradient Descent (SPGD) lattice form algorithms were used to model a headphone compensation filter and binaural Head-Related Transfer Function (HRTF), comparing the resulting IIR filters to equivalent FIR filters. Parameter studies on step-size coefficient and filter order were conducted to assess accuracy in both frequency and time domain.
The study found that both IIR filter forms reduced order length to 20% of the HRTF filter order and 40% of the compensation filter order, both within a 1 dB accuracy threshold in the magnitude response. This results in reduction in numerical operations of 60% for the HRTF filter and 20% for the headphone compensation filter.
This work demonstrates the that significant order reduction is possible using lattice form, gradient decent based adaptive filters. The exact reduction depends on the target filter and requires similar simulations and analysis to those used here.

Keywords: signal processing algorithms, adaptive filtering algorithms, time domain adaptive filters, IIR filters, filter order reduction, optimisation

Acknowledgements

I would like to thank my supervisor Jens for the very helpful advice and enthusiasm throughout this project. I also thank all of my colleagues and staff in the applied acoustics division for all the sharing of ideas and fun times over the last two years. Finally, thank you to my wife Alva, your support during this time has been immeasurable.

Alexander Lendon, Gothenburg 2025

Declaration of AI usage

AI tools were used in elements of the work of this thesis. Such uses were, generation of formatting settings for plot formatting, LaTeX config, creation of productivity tools. No report writing or code for the main work of the thesis was generated using AI.

List of acronyms

ARMA Auto Regressive Moving Average
DSP Digital Signal Processing
FIR Finite Impulse Response
GD Gradient Descent
HATO head above torso orientation
HpCF Headphone Compensation Filter
HRIR Head-Related Impulse Response
HRTF Head-Related Transfer Function
IIR Infinite Impulse Response
IR Impulse Response
LMS Least Mean Squares
PDF Probability Density Function
RLS Recursive Least Squares
SoS Series Second Order Sections
SPGD Simplified Partial Gradient Descent

Nomenclature

Below is the nomenclature of indices, sets, parameters, and variables that have been used throughout this thesis.

Parameters

μ	Step-size coefficient
N	Number of iterations
M	Filter order

Variables

$u(n)$	input signal sample at step n
$y(n)$	target output signal sample at step n
$\hat{y}(n)$	adaptive filter output signal sample at step n
$e(n)$	error sample at step n $y(n) - \hat{y}(n)$
$H(z)$	transfer function in z domain
$B(z)$	'b' coefficients polynomial expression in z domain
$A(z)$	'a' coefficients polynomial expression in z domain
b_k	k^{th} b coefficient of Direct Form filter
a_k	k^{th} a coefficient of Direct Form filter
ν_k	k^{th} ν coefficient of Lattice Form filter
θ_k	k^{th} θ coefficient of Lattice Form filter
∇_{coeff}	error gradient residual of a coefficient
ξ	Post filter state of lattice form filter
$\mathbf{T}_{dl}^{t}$	transformation matrix between b_k and ν_k

Contents

List of Algorithms

1

Introduction

In acoustics FIR filters are often used to represent transfer functions of acoustic systems. Often FIR filters are long and require a significant amount of compute resources when used in hardware, especially when the system of interest exhibits infinitely decaying response.[2],[1, Pref.] If FIR filters could be accurately represented using an IIR filter, the computational cost could potentially be reduced. This is important in, for example, wearable hardware, where computational resources are limited. IIR filters can be created by using optimization methods or, more specifically, adaptive filtering algorithms.

1.1 Background

The development of optimal filter design has progressed from direct block solutions, such as the Wiener solution, to computationally efficient iterative solutions such as Least Mean Squares (LMS) and Recursive Least Squares (RLS) solvers. The initial methods for these solvers were able to find optimal FIR filters and could be applied to IIR filters. However, solutions such as the IIR Wiener filter did not guarantee the stability of the filter. So FIR filter development became standard for most applications. With the improvement of computing speed, optimal IIR filters, which can guarantee stability, became the focus of research again.[2],[1, Pref.] Due to the standardisation of FIR filters in the field of acoustics, there are potentially overlooked applications where IIR filters could provide performance benefits. IIR filters may achieve similar performance with shorter filter order, resulting in reduced computational cost when the filter is in operation. This is important in hardware applications, such as wearables or VR/AR headsets, where power consumption must be minimized, or where other processes are highly demanding on processors. This work concerns the implementation, testing, and analysis of two adaptive IIR filter structures, Direct Form Modified Gradient Descent and Lattice Form Simplified Partial Gradient Descent, applied to two applications where FIR filters are a standard.

1.2 Aim

This study set out to better understand the performance of adaptive IIR filters when used to model an existing FIR filter. This is done by studying the effect of filter

design parameters such as the step-size coefficient and filter order, as well as the filter structure, and comparing when used in two application cases.

1.3 Research questions

- How does the choice between direct form and lattice form filter structure affect the performance of the resulting filter when estimating HRTF and Headphone Compensation Filter?
- How does the choice of step-size factor affect the performance of the resulting filter when estimating HRTF and Headphone Compensation Filter with an undermodelled adaptive filter?
- How does the choice of filter order affect the performance of the resulting filter when estimating HRTF and Headphone Compensation Filter?

1.4 Scope and Limitations

One lattice form and one direct form adaptive filter algorithm were selected from [1] to compare their performance. In both cases, an algorithm is chosen which reduced the per-step computational complexity which leads to faster convergence time. For the direct form filter the chosen algorithm is a modified gradient descent and for the lattice form the chosen algorithm is a simplified partial gradient descent. The headphone compensation filter and an HRTF are chosen to model because these filters are frequently used in spatial audio applications, including wearable devices where computational resources are limited.

1.5 Thesis outline

The thesis begins with a presentation of relevant background theory. A short summary of the concept of optimisation is presented before moving through signals, filter structures and finally tying all of these together with the adaptive filter algorithms.

In the method section the systems that have been modelled are shown and discussed with relevance to the method. The format of the investigations are then presented, beginning with step-size investigation and followed by the minimum order investigation.

In the results section, the results of the step-size investigation and the minimum order investigation are plotted and described. Here also some comparisons are shown between FIR and IIR filters.

The discussion section provides analysis of the results, in relation to the research question which provide some points for the following conclusion section.

2

Theory

In the following section a presentation of the theory underlying adaptive filter technology is presented.

Adaptive filter algorithms utilise numerical optimisation methods in conjunction with audio filter structures. In the sphere of numerical optimisation and adaptive algorithms there are countless modifications made of existing algorithms which provide performance benefits in specific applications.

Broadly, numerical optimisation problems can be divided into two categories, discrete and continuous. Continuous optimisation problems have an infinite solution space as the input and output variables are continuous. Discrete optimisation problems have finite solution spaces, which may still be large, but the inputs and outputs must form a countable set. This thesis is concerned with continuous optimisation problems due to the inherent continuous nature of audio signals.

It is however difficult to discuss the optimisation algorithms behind adaptive filters without also presenting the impact of filter structures on the performance. Mathematically, filter structures provide intermediate calculation steps or filter recursion states which correspond to signals within the filter architecture.

The presented material is limited to a number of fundamental algorithms and then algorithms specifically applied to filter structures with specific examples that have been applied in the experimentation phase.

2.1 Optimisation

The practice of numerical optimisation is motivated by selection of the best point in a data space based upon a defined performance criterion or objective function. The setup of the performance criterion defines the abilities of optimisation algorithms at the highest level and the manipulation of this is what allows for the wide array of applications of optimisation solutions. Usually the objective function is some form or error criteria which is intended to be minimised to zero.[3, Ch. 1]

Solutions to such problems may be solvable directly through inverse matrix methods. This however, may not be possible as it is dependent on a number of factors. First all data must be available at time of solving, the system of interest must also be time-invariant, finally computational limitations may occur for high-order system

estimations and in cases of non-linearity in the solution space a direct solution may be impossible.

Where it is not possible to find a direct solution, for reasons of time-invariance or with limited computational capabilities, one may apply a block iterative solution where solutions are found for smaller blocks of the signal and iteratively updated.

In the case where solution complexity is high, systems are time-varying or data is available in an online setting, then a recursive algorithm may be applied to find the optimal solution over time.[4, Ch. 5]

In complex, high-order problem spaces often the solution space is non-convex. This presents issues with slow convergence at saddle points and convergence to local minima.[5] There are many algorithms developed to avoid these issues and improve performance. However, in the field of acoustic signal processing there are additional constraints added to the optimisation problem involving, phase response and stability.[6, Ch. 1][1, Ch. 1]

2.1.1 Gradient Descent Based Methods

Gradient based methods are based upon the principal idea of minimising the error between the output of an estimated and a target function or system, by iteratively updating the estimation based upon a calculated error gradient. When coefficients are updated, this results in a new error value. The gradient of change in error with respect to a each coefficient can then be calculated or approximated. The sign of that gradient indicates if the error was increased or decreased by that coefficient change. By then updating that coefficient in the negative gradient direction in the next step, the error is gradually moved towards a minimum point in the error space. Doing this simultaneously for all coefficients means that as time approaches infinity, a minimum error value could be reached.[7, Ch. 1]

Within gradient based methods are many of the commonly used FIR adaptive filter algorithms. The LMS algorithm is such a type of stochastic gradient descent algorithm, using a simplification for the gradient term it can reduce computational complexity or convergence time relative to the standard gradient descent. [7, Ch. 4]

A range of gradient based methods for IIR filter design have been summarised in [8]. These methods include linear programming (LP), least squares (LS), wieghted least squares (WLS), semidefinite programming (SP), Min-max design using iterative linear programming (ILP) and conic quadratic programming (CQP).[8]

Further derivatives of algorithms are possible which exhibit a range of qualities and trade-offs between, convergence speed, computational complexity and requirements on signal properties or availability of data. In this way adaptive filters may be designed specifically for the system of interest and desired performance required.

2.1.2 Other optimisation methods

Many other non-gradient based algorithms are available to design IIR filters. Not all methods are compatible as adaptive filters. The following methods have not been used in this work.

One other commonly used method other than LMS is the RLS method. This method uses the least squares function as the objective function and includes all past input and output information in the update formula, usually with a forgetting factor to make distant past information negligible.[7, Ch. 10]

The Gauss-newton method uses the mean square error as the objective function. The minimisation of this function is obtained by searching in the Newton direction using estimates of the inverse Hessian matrix and gradient vector.[7, Ch. 10]

The survey conducted in [8] summarises many optimisation based methods used for design of IIR filters, including non-gradient methods such as evolutionary algorithms. Evolutionary techniques are a branch of methods that perform global search, meaning that they are able to search in multiple directions from the first estimation selecting the best performing directions over time. Examples of such algorithms mentioned in the paper include artificial immune algorithm (AIA), particle swarm optimization (PSO) artificial bee colony (ABC) algorithm, cat swarm optimization (CSO), seeker optimization algorithm (SOA), harmony search algorithm (HSA) and modified imperialist competitive (MIC) were used to find lower order IIR filters. Although the algorithms were successful in finding a valid filter in all cases, the phase responses of the solution were not linear and error due to quantisation of filter coefficients were also present.[8]

In [9] a deep-optimisation method was used to creater IIR filters for equalisation of a MIMO system of multiple loudspeakers and multiple listening positions in a room. The proposed method names BiasNet was implemented and computed coefficients for a cascade of Series Second Order Sections (SoS) of the desired order.

2.2 Digital Audio Signals

Gaussian white noise is used in this work as input signal in system identification problems using adaptive filters. In this section digital signals are explained and defined. The following definitions are taken from [10, Ch. 2].

Digital signals are discretised in time. This is opposed to continuous time signals which are the concern of analogue signal processing circuits. This work will only consider design of signal processing algorithms which considers discrete time signals, with a sample represented as:

$$u(n) \qquad \text{for } k = 0, \pm 1, \pm 2, \ldots$$

Where k is the sample step at time $t = \frac{k}{f_s}$ and f_s is the sample frequency.

2.2.1 Deterministic Signals

Deterministic signals are made up of combinations of periodic elements and their behaviour is known and predictable. There exist optimal filter solutions for systems with deterministic signals which utilise autocovariance functions or Z-transform models. While deterministic signals are of use in some system identification problems such as the sweep deconvolution method, in this thesis stochastic methods are used which require stochastic signals.[10, Ch. 2]

2.2.2 Stochastic Signals

There are signals, for example Gaussian white noise, where given the current and past samples, one can not predict the next sample. One can however give a probability that it will lie within certain bounds. Taking Gaussian white noise as example, the Gaussian Probability Density Function (PDF) (2.1) describes random signals with a bell curve distribution, centred around a mean value.

$$p(u) = \frac{1}{\sigma\sqrt{2\pi}} e^{\frac{1}{2}(\frac{u-\mu}{\sigma})^2} \tag{2.1}$$

where σ is the standard deviation and μ is the sample mean.[7, Ch. 2]
The moment generating function in (2.2) can be used to characterise a distribution.

$$E[u^n(n)] = \sigma^n = \sum_{k=-\infty}^{\infty} u(n)^n p(u(n)) \tag{2.2}$$

For $n = 1$ the sample mean μ is found by the function. The variance σ^2 is found using $n = 2$. $n = 3$ characterises the skewness and and $n = 4$, the Kurtosis, measures the tails and flatness of the top of the distribution. However, when considering a Gaussian distribution, higher orders of this measure ($n = 3, 4$) give zero values so they are not relevant in this work.[10, Ch. 2]

The sample mean for N samples or expectation of the signal is therefore:

$$E[u(n)] = \mu = \frac{1}{N} \sum_{k=1}^{N} u(n) \tag{2.3}$$

For $\mu = 0$ the variance is given by:

$$E[u^2(n)] = \sigma^2 = \frac{1}{N} \sum_{k=1}^{N} u(n)^2 \tag{2.4}$$

2.3 Filter Structure

In this work all adaptive filters investigated are defined as causal, linear, discrete-time, and time-variant. In general, adaptive filters are based upon time-invariant filter structures with the inclusion of some processing for coefficient updates[1, Ch.2].

The most common filter structure classifications are Direct form filters, Lattice form filters and Cascade filters. Different filter structures allow for equivalent filtering of a signal and can provide performance benefits such as reduced computational requirement or guaranteed filter stability.[1, Ch.2]

The filter behaviour may be characterised by a magnitude response in the frequency domain and impulse response in the time domain. The filter itself may be defined mathematically in a number of ways including Z-domain (frequency domain) transfer function, the time-domain difference equation[11, Ch 10.]. A causal, linear, time-invariant filter with an FIR depends only on past and present input values. The impulse response of this filter maps precisely to the coefficient values. The general form of an FIR filter is shown in (2.5).

A causal filter with a infinite impulse response IIR produces output which depends on past and present input values and past output values. Thus an IIR filter is always recursive. An IIR filter produces a magnitude response with higher frequency resolution than an FIR filter of equivalent order. This means it may represent a response with higher $\mathrm{dB\,Hz^{-1}}$ changes in the magnitude response. The general form of an IIR filter is shown in (2.6).

$$y(n) = \sum_{k=0}^{N} b_k u(n-k) = \sum_{k=0}^{N} h_k u(n-k) \tag{2.5}$$

$$\begin{aligned} \sum_{m=0}^{M} a_m y(n-m) &= \sum_{k=0}^{N} b_k u(n-k) \\ 1 \cdot y(n) &= \sum_{k=0}^{N} b_k u(n-k) - \sum_{m=1}^{M} a_m y(n-m) \end{aligned} \tag{2.6}$$

An adaptive filter is one which takes a desired or target signal and input signal and computes the error between the target and actual output. This is then applied using internal signals of the filter to compute regressor coefficients used in an update equation.

2.3.1 Direct Form

The direct form filter is the simplest filter structure available. The Direct Form I represents a circuit analogy of the transfer function in the Z-domain where z^n represents delay of n samples.

FIR

The FIR filter transfer function may be represented simply in the Z-domain by the polynomial expression shown in (2.7). The output of the filter in this form is shown

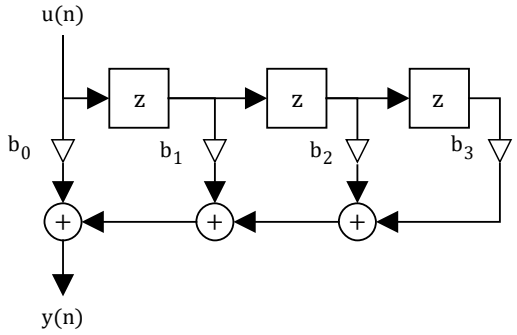

Figure 2.1: Signal flow block diagram, FIR Direct Form, $M = 3$

in (2.8). The output of the filter in the time domain is shown by the difference equation in (2.9).

$$\hat{H}(z) = B(z) = b_0 + b_1 z + \cdots + b_m z^M \tag{2.7}$$

$$\mathbf{Y} = \hat{H}(z) \cdot \mathbf{U} = B(z) \cdot \mathbf{U} \tag{2.8}$$

$$y(n) = \sum_{i=0}^{M} b_i u(n-i) \tag{2.9}$$

The corresponding block diagram is shown in Figure 2.1.

IIR

The IIR filter transfer function, in the Z-domain, is denoted by a rational function with coefficients corresponding to zeros in the numerator and coefficients corresponding to poles in the denominator.

$$\hat{H}(z) = \frac{B(z)}{A(z)} = \frac{b_0 + b_1 z + \cdots + b_M z^M}{1 + a_1 z + \cdots + a_N z^N} \tag{2.10}$$

$$\mathbf{Y} = \hat{H}(z) \cdot \mathbf{U} = \frac{B(z)}{A(z)} \cdot \mathbf{U} \tag{2.11}$$

The corresponding difference equation which results in the output of such a filter is given in (2.12).

$$y(n) = \sum_{i=0}^{M} b_i u(n-i) - \sum_{j=1}^{N} a_j y(n-j) \tag{2.12}$$

You may notice that the number of poles and zeros can differ if M or N are chosen such that $M \neq N$. This is known as an Auto Regressive Moving Average (ARMA) filter. Such filters do not provide any benefit in adaptive filtering applications. They effectively define a filter with order of $\max(M, N)$ with $|M - N|$ coefficients of value zero in either the poles or zeros polynomial. There is little justification for restriction

of the modelling capacity in this way so going forward IIR filters are defined by order M.[1, Ch. 2]

Formulating a system diagram corresponding to (2.12) for a filter order $M = 3$ results in the diagram shown in Figure 2.2. This is known as Direct Form I and is the first form of IIR filter. In Figure 2.2 a visual representation of the filter operations is seen.

The Direct Form I IIR filter opens up opportunities for simplification. By rearranging the structure as in Figure 2.3, three delay blocks may be omitted. This and other transformations in block flow diagrams are the basis for simplifications in many other filter structures, including adaptive filters[1, Ch. 2].

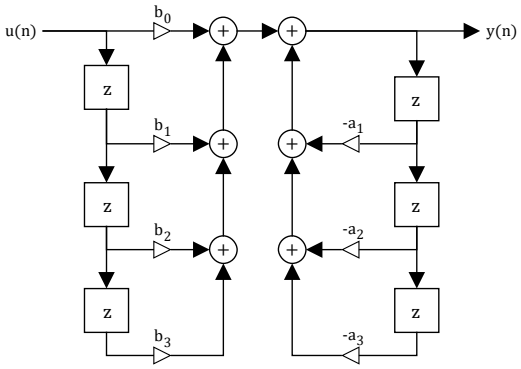

Figure 2.2: Signal flow block diagram, IIR Direct Form I, filter order M=3

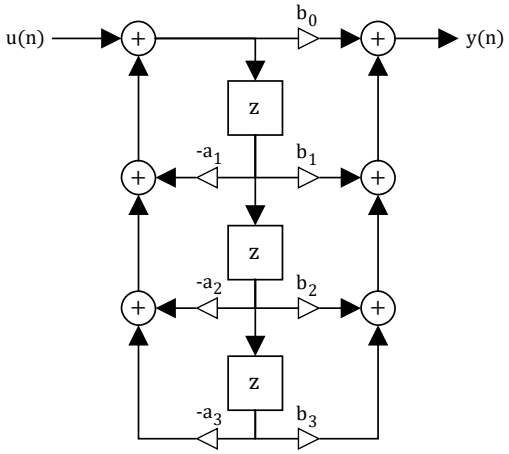

Figure 2.3: Signal flow block diagram, IIR Direct Form II, filter order M=3

2.3.2 Lattice Form

The lattice form filter structure is an alternative method of achieving a desired filter impulse response or magnitude spectrum. The lattice form filter comes as a result of applying the Gram-Schmidt Orthogonalisation Process on a set of input data.[6, Ch. 7] [12, Ch. 7]

By applying a transformation on the direct form filter coefficients, one may find the equivalent lattice filter representation, highly recursive filter structure is created. Lattice form filters exhibit desirable qualities such as an easy stability test, minimum or maximum phase representations, and possibility to change the filter order without recalculation of all coefficients.[1, Ch.2]

There are two recursion methods available for performing conversion between direct form and lattice form filter representations, the Schur Recursion and Levinson Durbin Recursion[1, Ch. 2,7].

Schur Recursion

The Schur Recursion and Levinson-Durbin Recursion, can be used to create a lattice structure mathematically. The algorithm solves a system of equations which exhibit a Toeplitz form, which is a feature of lattice signal paths.[13, Ch. 5][12, Ch. 3].

The result of the Schur algorithm is a set of reflection coefficients θ_k and, if applicable, ladder coefficients ν_k. In the context of a lattice filter structures in Figures 2.5,2.6 and 2.7, the recursive blocks, denoted by θ, can be represented by this recursion. This equivalence is shown in Figure 2.4 and a single step of this computation is shown in (2.13).

$$\begin{bmatrix} G_{k-1}(z) \\ F_k(z) \end{bmatrix} = \begin{bmatrix} \cos\theta_k, -\sin\theta_k \\ \sin\theta_k, \cos\theta_k \end{bmatrix} \begin{bmatrix} G_{k-1}(z) \\ F_k(z) \end{bmatrix} \tag{2.13}$$

The Schur recursion also provides a method for conversion between coefficients in lattice and direct form filter structures, shown in Algorithms 2.1 and 2.2. The objective of the transformation in either direction is to find the transformation matrix $\mathbf{T}_{dl}^t$ to convert between ν and $\mathbf{b}$ coefficients. During this process the coefficients θ and $\mathbf{a}$ are found at each step of the recursion from the $\mathbf{D}_M(z)$ matrix. [1, Ch. 2]

Algorithm 2.1 Conversion of direct form coefficients to lattice form coefficients using Schur Recursion[1]

Inputs:

$$A(z) \qquad \begin{bmatrix} a_1 & a_2 & \dots & a_M \end{bmatrix} \begin{bmatrix} z^1 & z^2 & \dots & z^m \end{bmatrix}^T$$

$$\mathbf{b} \qquad \begin{bmatrix} b_0 & b_1 & \dots & b_M \end{bmatrix}^T$$

Initialise: $D_M(z) = A(z), \hat{D}_M(z) = z^M A(z^{-1})$

for $k = M, M-1, \dots, 1$ **do**

$$\sin\theta_k = \frac{\hat{D}_k(0)}{D_k(0)}$$

$\triangleright$ take $\cos\theta_k$ positive

Apply Schur recursion, descending, to find the next values of $D_{k-1}(z)$ and $\hat{D}_{k-1}(z)$:

$$\begin{bmatrix} D_{k-1}(z) \\ \hat{D}_{k-1}(z) \end{bmatrix} = \frac{1}{cos\theta_k} \begin{bmatrix} 1 & -\sin\theta_k \\ -\sin\theta_k & 1 \end{bmatrix} \begin{bmatrix} D_k(z) \\ z\hat{D}_k(z) \end{bmatrix}$$

end for

Let: $\hat{\mathbf{d}}_\mathbf{k}$ be the $M+1$ element vector whose first $k+1$ elements contain the successive coefficients of the polynomial $\hat{D}_k(z)$,with the remaining $M-k$ elements set to zero. Then $[\hat{\mathbf{d}}_\mathbf{0}\hat{\mathbf{d}}_\mathbf{1}\cdots\hat{\mathbf{d}}_\mathbf{M}]$ builds an $(M+1)\times(M+1)$ matrix which is upper triangular. The tap parameters may then be obtained by the triangular backsolve.

$$\underbrace{\begin{bmatrix} \hat{\mathbf{d}}_\mathbf{0} & \hat{\mathbf{d}}_\mathbf{1} & \cdots & \hat{\mathbf{d}}_\mathbf{M} \end{bmatrix}}_{\triangleq \mathbf{T}_{dl}^t} \begin{bmatrix} \nu_0 \\ \nu_1 \\ \vdots \\ \nu_M \end{bmatrix} = \begin{bmatrix} b_0 \\ b_1 \\ \vdots \\ b_M \end{bmatrix}$$

Where $\mathbf{T}_{dl}^t$ is defined as the transformation matrix between $\{b_k\}$ and $\{\nu_k\}$.

Algorithm 2.2 Conversion of lattice form coefficients to direct form coefficients using Schur Recursion[1]

Inputs:

$$\theta(z) \qquad \begin{bmatrix}\theta_1 & \theta_2 & \dots & \theta_M\end{bmatrix} \begin{bmatrix}z^1 & z^2 & \dots & z^m\end{bmatrix}^T$$

$$\boldsymbol{\nu} \qquad \begin{bmatrix}\nu_0 & \nu_1 & \dots & \nu_M\end{bmatrix}^T$$

Initialise: $D_0 = \hat{D}_0 = \prod_{k=1}^{M} \cos\theta_k$

for $k = 1, 2, \dots, M$ **do**

Apply Schur recursion, ascending, to find the next values of $D_k(z)$ and $\hat{D}_k(z)$:

$$\begin{bmatrix} D_k(z) \\ \hat{D}_k(z) \end{bmatrix} = \frac{1}{\cos\theta_k} \begin{bmatrix} 1 & \sin\theta_k \\ \sin\theta_k & 1 \end{bmatrix} \begin{bmatrix} D_{k-1}(z) \\ z\hat{D}_{k-1}(z) \end{bmatrix}$$

end for

Let: $\hat{\mathbf{d}}_\mathbf{k}$ be the $M+1$ element vector whose first $k+1$ elements contain the successive coefficients of the polynomial $\hat{D}_k(z)$,with the remaining $M-k$ elements set to zero. Then $[\hat{\mathbf{d}}_\mathbf{0}\hat{\mathbf{d}}_\mathbf{1}\cdots\hat{\mathbf{d}}_\mathbf{M}]$ builds an $(M+1)\times(M+1)$ matrix which is upper triangular. The tap parameters may then be obtained by the multiplying the matrix.

$$\underbrace{\begin{bmatrix}\hat{\mathbf{d}}_\mathbf{0} & \hat{\mathbf{d}}_\mathbf{1} & \cdots & \hat{\mathbf{d}}_\mathbf{M}\end{bmatrix}}_{\triangleq \mathbf{T}_{dl}^t} \begin{bmatrix}\nu_0 \\ \nu_1 \\ \vdots \\ \nu_M\end{bmatrix} = \begin{bmatrix} b_0 \\ b_1 \\ \vdots \\ b_M \end{bmatrix}$$

Where $\mathbf{T}_{dl}^t$ is defined as the transformation matrix between $\{b_k\}$ and $\{\nu_k\}$.

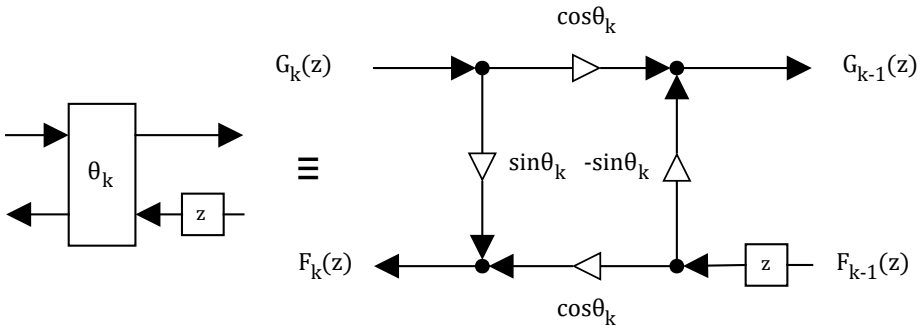

Figure 2.4: Signal flow block diagram, Schur Recursion Equivalence

Levinson-Durbin Recursion

The Levinson-Durbin Recursion is a method closely related to the Schur-recursion. Scaling the recursions $D_k(z)$ to make the first coefficient equal to one, and rearranging in ascending order gives the levinson durbin expressions [6]. In practice, this is equivalent to omitting the factor $\frac{1}{cos\theta_k}$ from the Schur recursion.

All Zero FIR

The difference equation for an M^{th} order all zero filter is equivalent to an FIR filter defined by (2.9) when coefficients are transformed by Schur recursion.

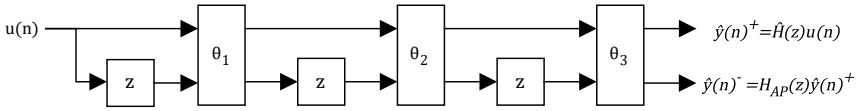

Figure 2.5: Signal flow block diagram, All Zero Lattice Form Filter, Order 3

All Pole IIR

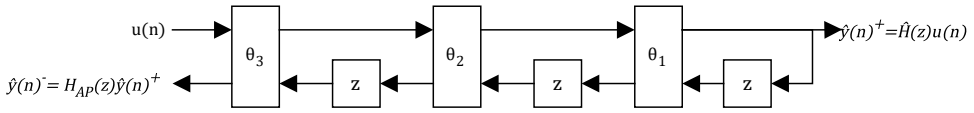

Figure 2.6: Signal flow block diagram, All Pole Lattice Form Filter, Order 3

Full IIR

A lattice filter that realises the general rational function, as in (2.10), may be implemented as a cascade of an all-pole filter $\frac{1}{A_M(z)}$ with an all zero filter $B_N(z)$. By observing Figures 2.5 and 2.6, it is more efficient to take out signals after delay blocks on the feed-backward chain of the all-pole filter.

By observing the signals labelled in the lattice filter structure of Figure 2.7 and using the Schur recursion defined in (2.13) a sum equation for the full lattice filter can be formulated as presented in (2.14).

$$\hat{y}(n) = \sum_{k=0}^{M} F_k \nu_k \tag{2.14}$$

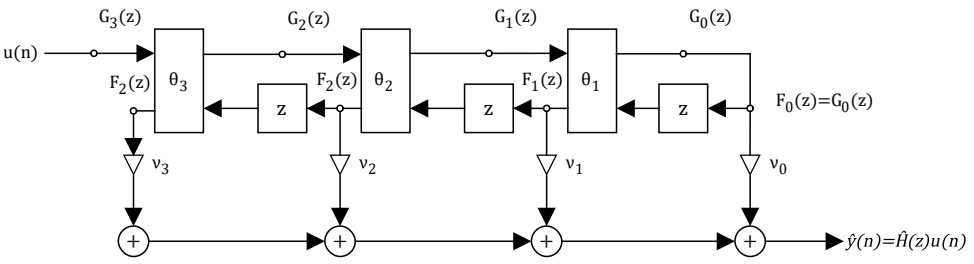

Figure 2.7: Signal flow block diagram, Tapped State Lattice Form Filter, Order 3

2.4 Adaptive Filter Algorithms

In this section the simplest form of direct and lattice form gradient descent algorithms are presented Algorithms 2.3 and 2.5 respectively. Then modified versions of each case which improve convergence properties are also presented for direct form in Algorithm 2.4 and lattice form in Algorithm 2.6. All algorithms are found in [1, Ch. 7].

Adaptive filtering algorithms use the same structure as time-invariant filters but with structures for regressor computation.[1, Ch.2]

2.4.1 Direct Form

The block diagram for the direct form gradient descent in Figure 2.8 corresponds to Algorithm 2.3 which is the basis for Algorithm 2.4. In [1, Ch. 7] comparison of convergence rate for the two algorithms is made. The Algorithm 2.4 is used in the studies of this work.

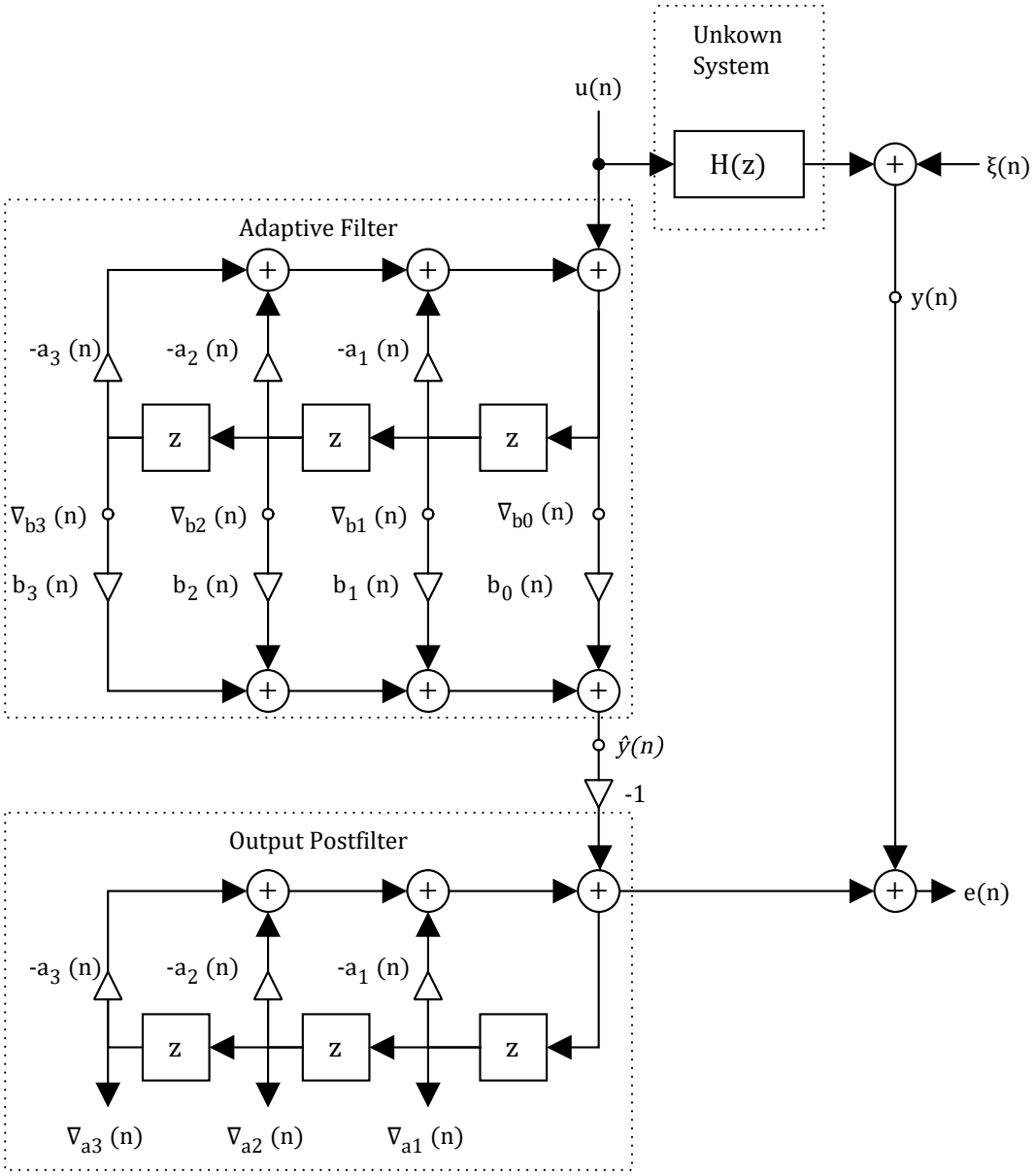

Figure 2.8: Signal flow block diagram depicting direct form adaptive filter [1, Ch. 7]

Gradient Descent

The direct form gradient descent algorithm is presented in Algorithm 2.3.

Algorithm 2.3 Direct Form Gradient Descent Algorithm[1]

Available at time n:
Filter states:

	$\nabla_{b_k}(n-1)$	$k = 0, 1, \ldots, M-1$ (Adaptive filter)
	$\nabla_{a_k}(n)$	$k = 1, 2 \ldots, M$ (Output postfilter)

Filter coefficients:

	$a_k(n)$	$k = 1, 2 \ldots, M$
	$b_k(n)$	$k = 0, 1, \ldots, M$

New data (signals):

	$u(n)$	(input sample)
	$y(n)$	(target sample)

Filter computations: ▷ *Example for $(M = 3)$
State recursion of adaptive filter: ▷ *

$$\begin{bmatrix} \nabla_{b_0}(n) \\ \nabla_{b_1}(n) \\ \nabla_{b_2}(n) \\ \nabla_{b_3}(n) \end{bmatrix} = \begin{bmatrix} -a_1(n) & -a_2(n) & -a_3(n) & 1 \\ 1 & 0 & 0 & 0 \\ 0 & 1 & 0 & 0 \\ 0 & 0 & 1 & 0 \end{bmatrix} \begin{bmatrix} \nabla_{b_0}(n-1) \\ \nabla_{b_1}(n-1) \\ \nabla_{b_2}(n-1) \\ u(n) \end{bmatrix}$$

Output sample $\hat{y}(n)$ and output error $e(n)$:

$$\hat{y}(n) = \sum_{k=0}^{M} b_k(n) \nabla_{b_k}(n)$$
$$e(n) = y(n) - \hat{y}(n)$$

Coefficient update:

$$b_k(n+1) = b_k(n) + \mu e(n) \nabla_{b_k}(n), \qquad k = 0, 1, \ldots, M$$
$$a_k(n+1) = a_k(n) + \mu e(n) \nabla_{a_k}(n), \qquad k = 1, 2, \ldots, M$$

State recursion of output postfilter: ▷ *

$$\begin{bmatrix} \nabla_{a_1}(n+1) \\ \nabla_{a_2}(n+1) \\ \nabla_{a_3}(n+1) \end{bmatrix} = \begin{bmatrix} -a_1(n) & -a_2(n) & -a_3(n) & 1 \\ 1 & 0 & 0 & 0 \\ 0 & 1 & 0 & 0 \end{bmatrix} \begin{bmatrix} \nabla_{a_1}(n) \\ \nabla_{a_2}(n) \\ \nabla_{a_3}(n) \\ -\hat{y}(n) \end{bmatrix}$$

Modified Gradient Descent

The modified gradient descent algorithm computes an output error after each a and b coefficient update. This increases the complexity of the algorithm but often results in a slightly improved convergence rate than the standard algorithm.[1, Ch. 7]

Algorithm 2.4 Direct Form Modified Gradient Descent Algorithm[1]

Available at time n:
Filter states:

$\nabla_{b_k}(n-1)$	$k = 0, 1, \ldots, M-1$	(Adaptive filter)
$\nabla_{a_k}(n)$	$k = 1, 2 \ldots, M$	(Output postfilter)

Filter coefficients:

$a_k(n)$	$k = 1, 2 \ldots, M$
$b_k(n)$	$k = 0, 1, \ldots, M$

New data (signals):

$u(n)$	(input sample)
$y(n)$	(target sample)

Filter computations: ▷ *Example for $(M = 3)$
Auxiliary signal in adaptive filter: ▷ *

$$x(n) = \begin{bmatrix} -a_3(n) & -a_2(n) & -a_1(n) & 1 \end{bmatrix} \begin{bmatrix} \nabla_{b_2}(n-1) \\ \nabla_{b_1}(n-1) \\ \nabla_{b_0}(n-1) \\ u(n) \end{bmatrix}$$

A priori output sample $\tilde{y}(n)$ and a priori output error $\tilde{e}(n)$: ▷ *

$$\tilde{y}(n) = \begin{bmatrix} b_3(n) & b_2(n) & b_1(n) & b_0(n) \end{bmatrix} \begin{bmatrix} \nabla_{b_2}(n-1) \\ \nabla_{b_1}(n-1) \\ \nabla_{b_0}(n-1) \\ x(n) \end{bmatrix}$$

$$\tilde{e}(n) = y(n) - \tilde{y}(n)$$

Feedback coefficient update:

$$a_k(n+1) = a_k(n) + \mu \tilde{e}(n) \nabla_{a_k}(n), \qquad k = 1, 2, \ldots, M$$

State recursion of adaptive filter: ▷ *

$$\begin{bmatrix} \nabla_{b_0}(n) \\ \nabla_{b_1}(n) \\ \nabla_{b_2}(n) \\ \nabla_{b_3}(n) \end{bmatrix} = \begin{bmatrix} -a_1(n+1) & -a_2(n+1) & -a_3(n+1) & 1 \\ 1 & 0 & 0 & 0 \\ 0 & 1 & 0 & 0 \\ 0 & 0 & 1 & 0 \end{bmatrix} \begin{bmatrix} \nabla_{b_0}(n-1) \\ \nabla_{b_1}(n-1) \\ \nabla_{b_2}(n-1) \\ u(n) \end{bmatrix}$$

A posteriori output sample $\hat{y}(n)$ and output error $e(n)$:

$$\hat{y}(n) = \sum_{k=0}^{M} b_k(n) \nabla_{b_k}(n)$$

$$e(n) = y(n) - \hat{y}(n)$$

Feed-forward coefficient update:

$$b_k(n+1) = b_k(n) + \mu e(n) \nabla_{b_k}(n), \qquad k = 0, 1, \ldots, M$$

State recursion of output postfilter: ▷ *

$$\begin{bmatrix} \nabla_{a_1}(n+1) \\ \nabla_{a_2}(n+1) \\ \nabla_{a_3}(n+1) \end{bmatrix} = \begin{bmatrix} -a_1(n+1) & -a_2(n+1) & -a_3(n+1) & 1 \\ 1 & 0 & 0 & 0 \\ 0 & 1 & 0 & 0 \end{bmatrix} \begin{bmatrix} \nabla_{a_1}(n) \\ \nabla_{a_2}(n) \\ \nabla_{a_3}(n) \\ -\hat{y}(n) \end{bmatrix}$$

2.4.2 Lattice Form

This section presents the adaptive lattice form filter structure, a basic gradient algorithm and a simplified modification that were used in the studies of this work. Much like the direct form adaptive filters, the adaptive lattice filter is built upon an IIR filter, using regressor circuits to process coefficient update computation. In the lattice filter, these regressor computers are taken out of the reflection coefficient recursive blocks. This is shown for a single case in Figure 2.9.

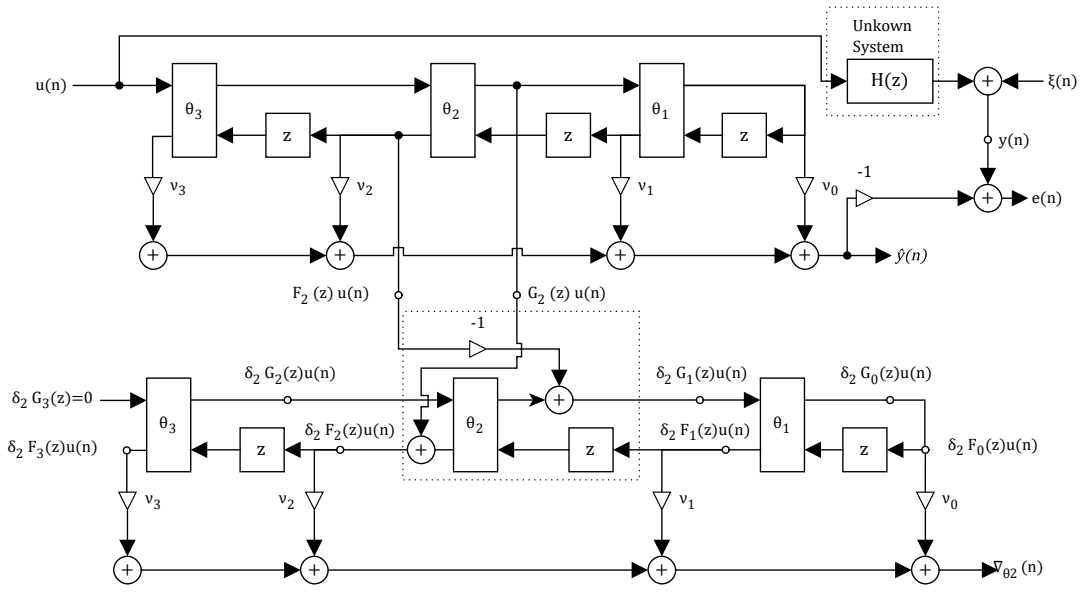

Figure 2.9: Single filtered regressor signal in an adaptive lattice filter with regressor states labelled [1, Ch. 7]

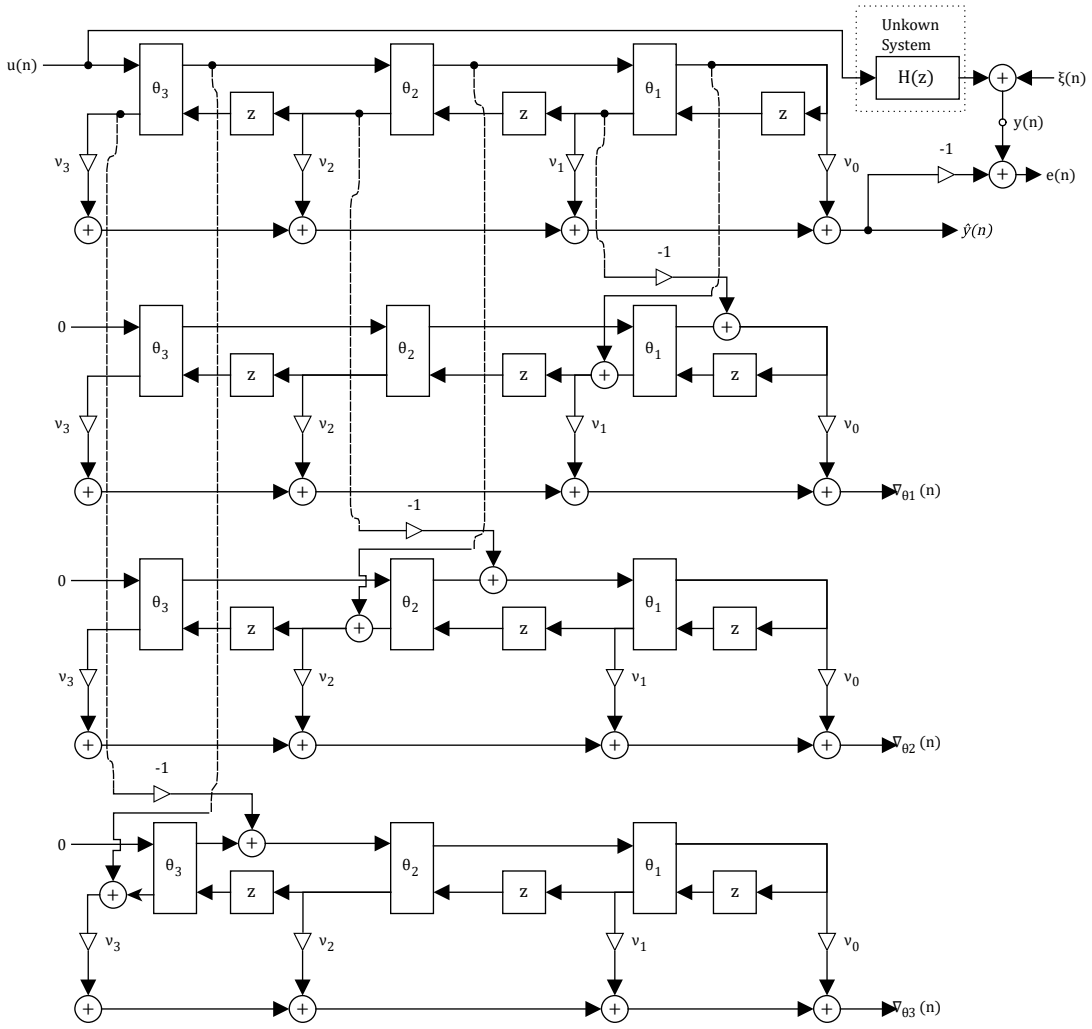

Figure 2.10: Signal flow block diagram, depicting a all filtered regressor signals in an adaptive lattice filter of order $M = 3$ [1, Ch. 7]

Gradient Descent

The Lattice Form, Gradient Descent algorithm is presented in Algorithm 2.5. The signal flow block diagram is given in Figure 2.10 with all filtered regressor circuits included. This algorithm is the basis for other modifications and simplifications of the adaptive gradient lattice filter structure. An investigation into their performance in simulated examples is made in [1, Ch. 7].

Algorithm 2.5 Lattice Gradient Descent Algorithm [1]

Available at time n:
Filter coefficients:

$$\begin{aligned} &\nu_k(n) && k = 0, 1 \ldots, M \\ &\theta_k(n) && k = 1, 2 \ldots, M \end{aligned}$$

Adaptive filter states:

$$\nabla_{\nu_k}(n-1) \qquad k = 0, 1, \ldots, M-1$$

$\triangleright$ ∇_{ν_M} computed but not stored

Post filter states:

$$\begin{aligned} &\xi_{k,l}(n-1) && k = 1, 2 \ldots, M \\ &&& k = 1, 2 \ldots, M \end{aligned}$$

$\xi_{k,M}(n)$ *computed but not stored*

New data (Signals):

$$\begin{aligned} &u(n) && \text{(input sample)} \\ &y(n) && \text{(target sample)} \end{aligned}$$

Adaptive filter computation:
let $g_M = u(n)$
for $k = M, M-1, \ldots, 1$ **do**

$$\begin{bmatrix} g_{k-1} \\ \nabla_{\nu_k}(n) \end{bmatrix} = \begin{bmatrix} \cos\theta_k(n) & -\sin\theta_k(n) \\ \sin\theta_k(n) & \cos\theta_k(n) \end{bmatrix} \begin{bmatrix} g_k \\ \nabla_{\nu_{k-1}}(n-1) \end{bmatrix}$$

end for

$$\nabla_{\nu_0}(n) = g_0$$

Adaptive filter output:

$$\hat{y}(n) = \sum_{k=0}^{M} \nu_k(n) \nabla_{\nu_k}(n)$$

Output error:

$$e(n) = y(n) - \hat{y}(n)$$

Post filter computation:
let $f_{k-1} = g_{k-1}$
for $k = 1, 2, \ldots, M$ **do**
  let $g_{k,M} = 0$
  for $l = M, M-1, \ldots, 1$ **do**
    if l=k **then**

$$\begin{bmatrix} g_{k,l-1} \\ \xi_{k,l}(n) \end{bmatrix} = \begin{bmatrix} \cos\theta_l(n) & -\sin\theta_l(n) \\ \sin\theta_l(n) & \cos\theta_l(n) \end{bmatrix} \begin{bmatrix} g_{k,l} \\ \nabla_{\xi_{k,l-1}}(n-1) \end{bmatrix} + \begin{bmatrix} -\nabla_{\nu_k}(n) \\ f_{k-1} \end{bmatrix}$$

    else

$$\begin{bmatrix} g_{k,l-1} \\ \xi_{k,l}(n) \end{bmatrix} = \begin{bmatrix} \cos\theta_l(n) & -\sin\theta_l(n) \\ \sin\theta_l(n) & \cos\theta_l(n) \end{bmatrix} \begin{bmatrix} g_{k,l} \\ \nabla_{\xi_{k,l-1}}(n-1) \end{bmatrix}$$

end if $\xi_{k,0} = g_{k,0}$
end for l
Filtered regressor signal:

$$\nabla_{\theta_k} = \sum_{l=0}^{M} \nu_l(n)\xi_{k,l}(n)$$

end for k
Coefficient updates:

$$\nu_k(n+1) = \nu_k(n) + \mu e(n)\nabla_{\nu_k}(n), \qquad k = 0, 1, \ldots, M;$$

$$\theta_k(n+1) = \theta_k(n) + \mu e(n)\nabla_{\theta_k}(n), \qquad k = 1, 2, \ldots, M;$$

Test Stability:
for $k = 1, 2, \ldots, M$ **do**
if $|\theta_k(n+1)| > \frac{\pi}{2}$ **then**
set $\theta_k(n+1) = \theta_k(n)$
end if
end for

Simplified Partial Gradient Descent

The Lattice Form, Simplified Partial Gradient Descent algorithm is presented in Algorithm 2.6. This is the algorithm that were used in the work for testing with lattice filters.

Algorithm 2.6 Lattice Simplified Partial Gradient Descent Algorithm [1]

Available at time n:
Filter coefficients:

$$\begin{aligned} &\nu_k(n) && k = 0, 1 \ldots, M \\ &\theta_k(n) && k = 1, 2 \ldots, M \end{aligned}$$

Adaptive filter states:

$$\nabla_{\nu_k}(n-1) \qquad k = 0, 1, \ldots, M-1$$

▷ ∇_{ν_M} computed but not stored

Post filter states:

$$\xi_k(n-1) \qquad k = 1, 2 \ldots, M$$

New data (Signals):

$$\begin{aligned} &u(n) && \text{(input sample)} \\ &y(n) && \text{(target sample)} \end{aligned}$$

Adaptive filter computation:
let $g_M = u(n)$
for $k = M, M-1, \ldots, 1$ **do** ▷ g_{k-1} may overwrite g_k

$$\begin{bmatrix} g_{k-1} \\ \nabla_{\nu_k}(n) \end{bmatrix} = \begin{bmatrix} \cos\theta_k(n) & -\sin\theta_k(n) \\ \sin\theta_k(n) & \cos\theta_k(n) \end{bmatrix} \begin{bmatrix} g_k \\ \nabla_{\nu_{k-1}}(n-1) \end{bmatrix}$$

end for

$$\nabla_{\nu_0}(n) = g_0$$

Adaptive filter output:

$$\hat{y}(n) = \sum_{k=0}^{M} \nu_k(n) \nabla_{\nu_k}(n)$$

Output error:

$$e(n) = y(n) - \hat{y}(n)$$

Filtered regressors computation:
let $\gamma_M = 1$
for $k = M, M-1, \ldots, 1$ **do** ▷ γ_{k-1} may overwrite γ_k

$$\begin{aligned} \nabla_{\theta_k} &= \gamma_K \xi_{k-1}(n) \\ \gamma_{k-1} &= \gamma_k \cos\theta_k(n) \end{aligned}$$

end for
Coefficient updates:

$$\begin{aligned} \nu_k(n+1) &= \nu_k(n) + \mu e(n) \nabla_{\nu_k}(n), && k = 0, 1, \ldots, M; \\ \theta_k(n+1) &= \theta_k(n) + \mu e(n) \nabla_{\theta_k}(n), && k = 1, 2, \ldots, M; \end{aligned}$$

Test Stability:
for $k = 1, 2, \ldots, M$ **do**
  if $|\theta_k(n+1)| > \frac{\pi}{2}$ **then**
    set $\theta_k(n+1) = \theta_k(n)$
  end if
end for
Post filter computation:
let temp $= -\hat{y}(n)$
for $k = M, \ldots, 2, 1$ **do** ▷ "temp" is overwritten

$$\begin{bmatrix} \text{temp} \\ \xi_k(n+1) \end{bmatrix} = \begin{bmatrix} \cos\theta_k(n+1) & -\sin\theta_k(n+1) \\ \sin\theta_k(n+1) & \cos\theta_k(n+1) \end{bmatrix} \begin{bmatrix} \text{temp} \\ \xi_{k-1}(n) \end{bmatrix}$$

end for

$$\xi_0(n+1) = \text{temp}$$

2.5 Adaptive Filter Performance

This section explains some parameters that can define the performance of an adaptive filter.

2.5.1 Computational Complexity

Observing the filter block diagrams in Figures 2.2-2.7, highlights an important aspect of digital filters where hardware implementation is considered. Each coefficient multiplication and addition (accumulation) represents a computation or hardware that must be assigned to the audio processor hardware. Additionally each delay block also represents hardware which must be implemented. Algorithms which provide convergence speed or accuracy improvements often do so with cost increase in computational complexity.

2.5.2 Fixed Point Value Sensitivity

In hardware there is a limited accuracy for very small decimal values dependent on the allocated word length for floating point values. This can cause errors in rounding where values require greater precision than is provided in the hardware.

As poles and zeros approach the unit circle in the Z-transform representation, value changes in coefficients affect the pole and zero positions at a different rate than in other positions. In a direct form filter,the pole and zero positions are highly sensitive to the rounding of coefficient values when close to the unit circle. Comparatively, in lattice filters the pole and zero positions are less sensitive towards the round-off errors. [1, Ch. 2]

2.5.3 Convergence Speed

For gradient descent methods, the rate of convergence is determined by the order of complexity of the algorithm, the step-size factor and the nature of the system the

algorithm is solving.[3]

The computational complexity affects the computational resources needed for adaption. It defines the per-step computation time and in real-time operation can set an upper limit on available sample rates when computational resources are limited. This does not necessarily relate to the amount of required iterations to convergence as this depends on the efficacy of the operations, not simply the complexity.

On the efficacy of algorithms, some adaptive filter algorithms are more sensitive to large adjustments of coefficient values, in some cases becoming unstable with large updates. In unstable cases it is important to have control over the convergence rate by implementing the step-size factor μ, sometimes called the convergence factor. Whilst there are methods for estimating a theoretical maximum step-size factor for a given problem space, they produce a bound which must still be validated with simulation. Therefore the final choice of step-size factorμ is most often made through the use of simulations.[7, Ch. 2][1, Ch. 2]

2.5.4 Stability

In IIR filtering a key design issue is filter stability. It is therefore essential to have a test or guarantee for stability, built-in to any adaptive filter algorithm. Unfortunately the direct form IIR filter structure does not easily give such a solution. The lattice filter structure however does and a stability test for direct form filters requires conversion of the coefficients into lattice form. For an online implementation this is impractical and extremely computationally costly. For this reason it makes practical sense to just implement a lattice form adaptive filter. The stability condition of a lattice filter requires that the reflection coefficients are kept with a modulus less than one $\sin\theta < 1$. [1, Ch. 2]

2.6 Applications

Adaptive filters are a necessity for applications involving non-stationary systems or tracking of non-stationary signals such as in speech encoding. They are also useful in filter design applications where the desired filter structure is recursive and as such cannot easily be solved by simple matrix methods.

In this work the adaptive filter is used as a filter design tool in a system identification problem. Here the algorithms are used as a means to model functions with an IIR filter which are typically created using an FIR filter. Typically, IIR filters are able to represent a similar magnitude response with a reduced filter order when compared with the original FIR filter. The advantage of this is a reduced computational cost during operation of the filter.

2.6.1 System Identification

System identification is but one of many applications of adaptive filters. Below some interesting acoustic systems which are typically represented by FIR filters are

presented. There is interest in modelling such filters with greatly reduced order IIR filters due to their use in modern wearable technologies such are AR/VR headsets.

Headphone Compensation Filter

Most consumer headphones do not have a suitably flat magnitude response to be able to accurately recreate binaural audio signals. Therefore it is a requirement to create filters which compensate for this behaviour and provide a suitably flat response to then apply and binaural processing filters to the signal.

A headphone compensation filter is one such filter for a specific headphone set. By measuring the transfer function for each headphone can, and inverting the resulting magnitude response and the result is a simple compensation filter.

The headphone compensation filters provided in [14] consist of an inverted headphone magnitude function and a regularisation function to reduce the magnitude of any large, sharp peaks.

HRTF

A HRTF is a transfer function which describes the propagation of sound from a source position to both ears. HRTF functions are usually defined for a fixed radius from head centre (m), azimuth (ϕ°), elevation (θ°) and head above torso orientation (HATO) (HATO°).[14] A demonstration of azimuth is shown in Figure 2.11, the elevation follows naturally as the same in the vertical plane and HATO is the case where the torso remains forward facing and the head is turned by some angle. HRTF functions may be provided in the form of a Head-Related Impulse Response (HRIR), which can be implemented as an FIR filter of the same length with coefficients equal to each sample of the Impulse Response (IR).

When modelling an HRTF, it is possible to assume minimum-phase functions for the filter magnitude response with inter-aural phase differences approximated by a simple time delay. [15]

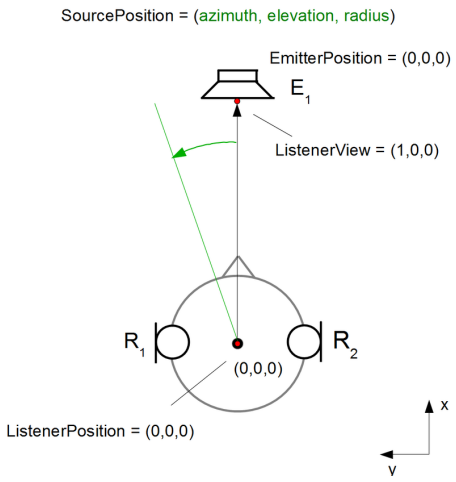

Figure 2.11: HRTF Azimuth [16]

3

Methods

This chapter introduces the methods used for analysis of adaptive filters that were presented in Section 2. The relevant performance criteria for adaptive filters depends on the intended application of the filter, both in terms of the hardware used and the systems that it is applied to.

Often filters used in signal processing applications are represented using FIR filters due filter stability and a simplified estimation procedure when calculating the filter coefficients. Such FIR filters are often in the order of hundreds of coefficients. By representing the same filter with an IIR filter of greatly reduced order,the resulting computational cost during operation would also be reduced. Additionally, in an adaptive context, when convergence speed is sufficiently fast, this would represent a significant reduction in processing requirements.

The performance criteria relevant in the context of this thesis are therefore; the convergence time, absolute convergence error and the accuracy estimated filter, represented by divergence from the target filter magnitude function. These criteria are used to assess a suitable minimum filter order for each filter application and adaptive filter structure.

3.1 Systems

Each case investigated in this work is a stationary system identification problem. The systems of interest are Headphone Compensation Filter (HpCF) and a measured HRIR. All system IRs are sourced from [14].

Heaphone Impulse Response

Figure 3.1 shows the measured IR and magnitude spectrum of a left headphone on the Beyerdynamic DT770 Pro 32 Ohm for which a compensation filter was created.

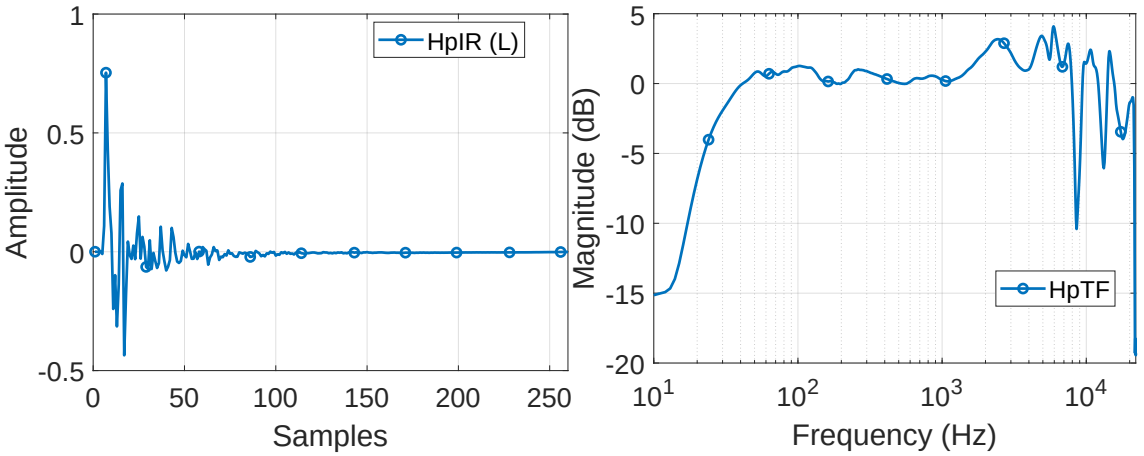

(a) Impulse Response (Left Ear)

(b) Headphone Transfer Function (Left Ear)

Figure 3.1: IR and Magnitude Spectrum for a Beyerdynamic DT770 Pro 32 Ohm

Headphone Compensation Filter

Figure 3.2 shows the impulse response and magnitude spectrum for the headphone compensation filter. This includes a regularisation function which reduces the magnitude of negative peaks seen around 10 kHz in Figure 3.1a. For identification of this system using an IIR filter a minimum phase representation was used.

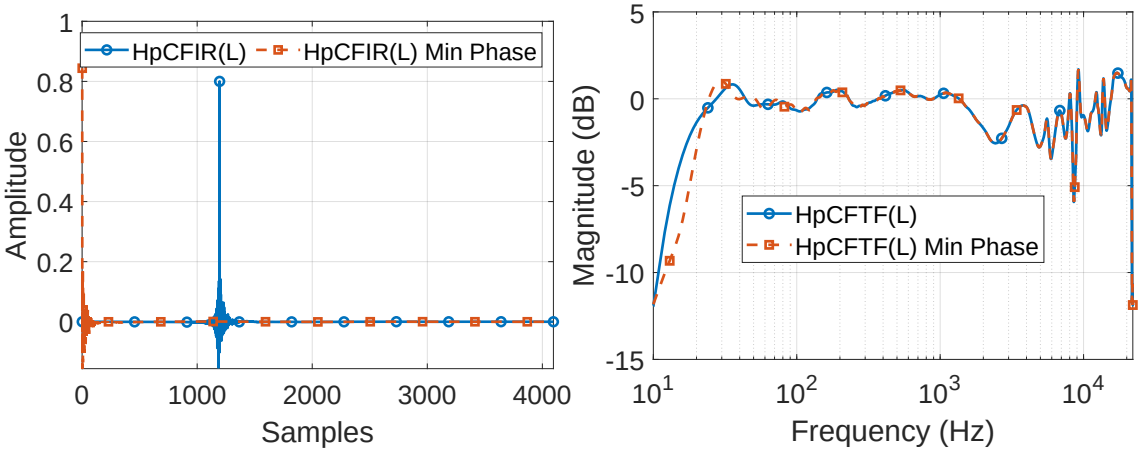

(a) Impulse Response (Left Ear)

(b) Magnitude Spectrum (Left Ear)

Figure 3.2: IR and Magnitude Spectrum for a HpCF for Beyerdynamic DT770 Pro 32 Ohm, measured and minimum phase representation

Head-Related Impulse Response

Figure 3.3 shows the impulse response and magnitude spectrum for the HRIR. Here again an minimum phase representation was used for identification with an adaptive IIR filter. The orientation of HATO 50°, azimuth 0° and elevation 0° was chosen to to demonstrate the ipsi-contra lateral differences in impulse response. In this case the right ear channel is the ipsilateral and the left each channel the contralateral channel. The inter-aural time delay gap is shown in the measured IR case in Figure 3.3a, this is not present in the minimum phase representation. When using minimum phase representations the inter-aural time delay is simply added back post estimation as a simple delay. The effect of the shadow resulting blocking of the transfer path by the head is evident in both Figures 3.3a and 3.3b where the contralateral channel is reduced in amplitude increasingly in the high frequency range.

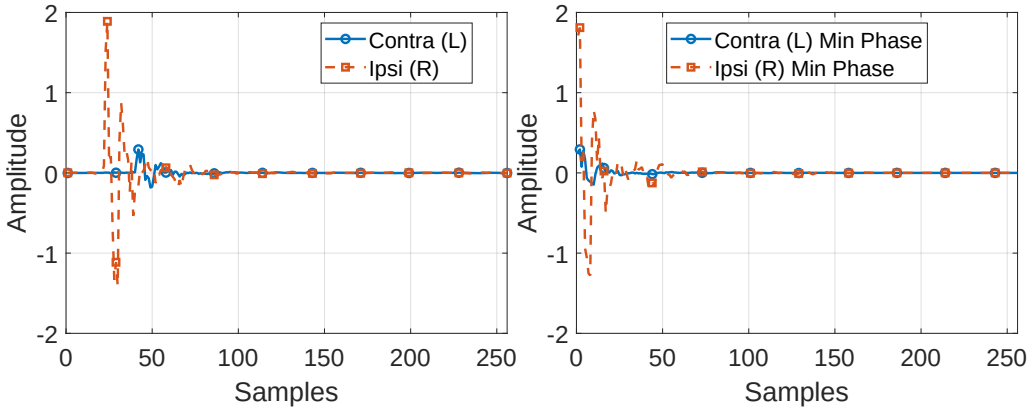

(a) HRIR (Ipsi- & Contra- Lateral)

(b) HRIR Minimum Phase (Ipsi- & Contra- Lateral)

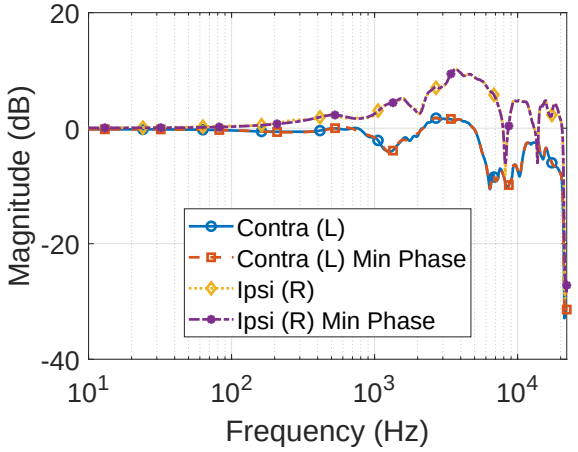

(c) HRTF (Ipsi- & Contra- Lateral)

Figure 3.3: HRIR and HRTF, for HATO 50, $\phi = 0°$,$\theta = 0°$ measured and minimum phase representation

3.2 System Identification

The fastest converging adaptive algorithms from each filter form were used for the system identification. For direct form, the modified gradient descent algorithm, listed in Algorithm 2.4 (Direct Form Modified Gradient Descent) was used. For lattice form the simplified proximal gradient descent algorithm listed in Algorithm 2.6 (Lattice Form Simplified Proximal Gradient Descent) was used.

Each algorithm takes input of filter order (M), input signal ($\mathbf{x}$), output (target) signal ($\mathbf{y}$), iterations (n) and step-size factor (μ). The input signal was white Gaussian noise with a power level of $-20\,\mathrm{dB\,W}$. The output signal was calculated by performing a convolution between the input signal and the impulse response of the system of interest.

3.2.1 Finding a Performance Baseline

To get an idea of the level of improvement of the generated IIR filters a baseline result can be found from FIR filters. Apart from comparing the modelled IIR against the original FIR comparison can be made against the a truncated FIR, cut in length to match the order M of the IIR. If the performance of the modelled IIR filters does not improve upon the truncated FIR filters, then it is clear in such a case that implementing an IIR filter would be obsolete. The filter orders investigated in this way are listed in Table 3.1. A selection of truncated FIR filters were compared directly with corresponding filters computed in the minimum order investigation.

	M (Original)	M (High)	M (Low)
HpCFIR	4096	100,220*,460,1000*	20*,50,70,100*
HRIR	256	20,50*,70,100*	4*, 10, 14, 20*

Table 3.1: FIR orders cut form original length
*Results compared with IIR estimations of same order

3.2.2 Step-size Investigation

The effect of step-size was investigated and the parameters selected for each system are shown in 3.2. As discussed in Section 2.5, a minimised step-size allows for a higher degree of accuracy upon convergence, or less variance in the converged results. This comes at a cost of slower convergence. Larger step-size results in a faster convergence with higher variance in the result. In some adaptive filter structures which are prone to instability, a larger step-size factor may result in instability during operation.[1][6]. Therefore for operation of adaptive filters it is of interest to find the maximum stable step size.

System	M	μ	n
HpCFIR	100	1	3.5×10^5
		1×10^{-1}	3.5×10^4
		1×10^{-2}	7×10^4
		1×10^{-3}	7×10^5
		1×10^{-4}	3.528×10^6
HRIR	20	1	3.5×10^4
		1×10^{-1}	3.5×10^4
		1×10^{-2}	7×10^4
		1×10^{-3}	7×10^5
		1×10^{-4}	3.528×10^6

Table 3.2: Adaptive filter parameters for step-size study

When investigating the effect of filter order M, the same step-size factor and number of iterations n were used in all cases. Both were selected to reach convergence in all cases. Computing the algorithms for a number of iterations beyond convergence does affect the resulting filter, but there is no overall improvement with regards to the error. For each algorithm the same filter orders were investigated to allow for comparison.

The filter order (M), step-size (μ) and number of iterations (n), used in the step-size study are shown in Table 3.2

3.2.3 Minimum Order Investigation

The key benefit of implementing IIR filters is the reduction in required filter order. Therefore, it is of interest to assess the effect of filter order on the performance of the filters.

The universal parameters for minimum order study are shown in Table 3.3. The filter orders used in the minimum order study are shown in Table 3.4. A range of order lengths were selected relative to the original length of the target impulse response. both cases have filters which extend up to roughly half the length of the target IR and as down as low as roughly 1-2% of the target IR lengths. For the headphone compensation filter the largest filter orders were computed with lattice filter only due to issues with divergence in the direct form filter when computing such large filters.

μ	n^*
0.03	3.5×10^4

Table 3.3: Universally applied adaptive filter parameters
* Very high order lattice computations (HpCFIR lattice only) were run until convergence, requiring orders of magnitude more iterations than the value listed here

	M (High)	M (Low)	M (Lattice Only)
HpCFIR	100,220,460,1000	20,50,70,100	1000,1600,2000,2300
HRIR	20,50,70,100	4, 10, 14, 20	

Table 3.4: Filter orders computed for the minimum order investigations

A comparison is made of estimations of the ipsi- and contra- lateral HRIRs. The filter input parameters are lsited in 3.5

	M	n	mu
HRIR(Ipsi&Contra)	150	1e5	0.03

Table 3.5: Comparison of ipsilateral and contralateral filter estimations

4

Results

In this section results for the studies conducted are presented. First, results from step-size investigation conducted on both the headphone compensation filter and HRIR are presented, in this study both lattice and direct filters were used in estimation. Next the results from the minimum required order study are presented. Here again both the headphone compensation filter and HRIR were estimated with lattice and direct form filters. Additionally, the effect of implementing a reduced order FIR for each system is presented.

There are a total of five plots for each test and will be provided in this order:

- Magnitude Spectrum of target and estimated filters

$$(H_{\text{est}}, (f)H_{\text{target}}(f))$$

- Deviation of estimated filter spectra from target magnitude spectrum

$$H_{\text{dev}}(f) = H_{\text{est}}(f) - H_{\text{target}}(f)$$

- First peak of impulse response

$$(H_{\text{est}}(t), H_{\text{target}}(t)), \quad t = 1, 2, \ldots, 100$$

- Absolute of impulse response plotted on logarithmic Y axis

$$(|H_{\text{est}}(t)|, |H_{\text{target}}(t)|)$$

- Output error over iterations, smoothed with moving mean size k.

$$e(n) = Y(n) - \hat{Y}(n)$$

Where generically H is a filter in the domains; frequency (f), time (t), corresponding to magnitude spectrum and impulse response respectively. Additionally target filter output Y, estimated filter output $\hat{Y}$ and error e at iteration step (n).

In each case some plots may be omitted where they do not provide further insight or are indistinguishable to another case, for example this often occurs between the lattice and direct form solutions.

4.1 Step-size Investigation

The results for the step-size investigation for headphone compensation filter and the HRTF are presented below.

4.1.1 Headphone Compensation Filter Estimation

In Figure 4.1 are the results of tests listed in 3.2 for estimation of a headphone compensation filter with a direct form IIR filter representation.

Figure 4.1a shows the final magnitude response of the estimated filters and Figure 4.1b shows the deviation of the estimated filter magnitude response from the target magnitude response. Here, all filters that converged exhibit similar performance. The best performing step-size factor was $\mu = 0.1$ which better captured the sharp peaks and sub-peaks in the region around 10 kHz. Figure 4.1c shows the magnitude of the whole impulse response for each estimation. It shows that the step-size factor inversely affects the gradient of the exponential decay. Although the rate of the decay generally increases with a decreasing step-size factor, there is no precise relationship observable form this plot. The curve of $\mu = 0.1$ shows a periodic pattern of sub-peaks, repeating every 800-900 samples. This is difficult to define in the magnitude representation of the plot as it is likely where values are crossing zero.

Figure 4.1d shows the adaptive filter output error over iterations. For step-size factors $\mu = [1 \times 10^{-2}, 1 \times 10^{-3}, 1 \times 10^{-4}]$, a similar convergence error average is reached. For these three cases, step-size factors also demonstrate that decreasing μ by one order of magnitude results in an increase, by one order of magnitude, in required iterations for convergence. The cases where $\mu = [0.1, 1]$ show unexpected behaviour, with reduced starting error values and less stable results when approaching convergence. In the case where $\mu = 1$ the filter became unstable and the result diverged, leading to infinite valued filter coefficients.

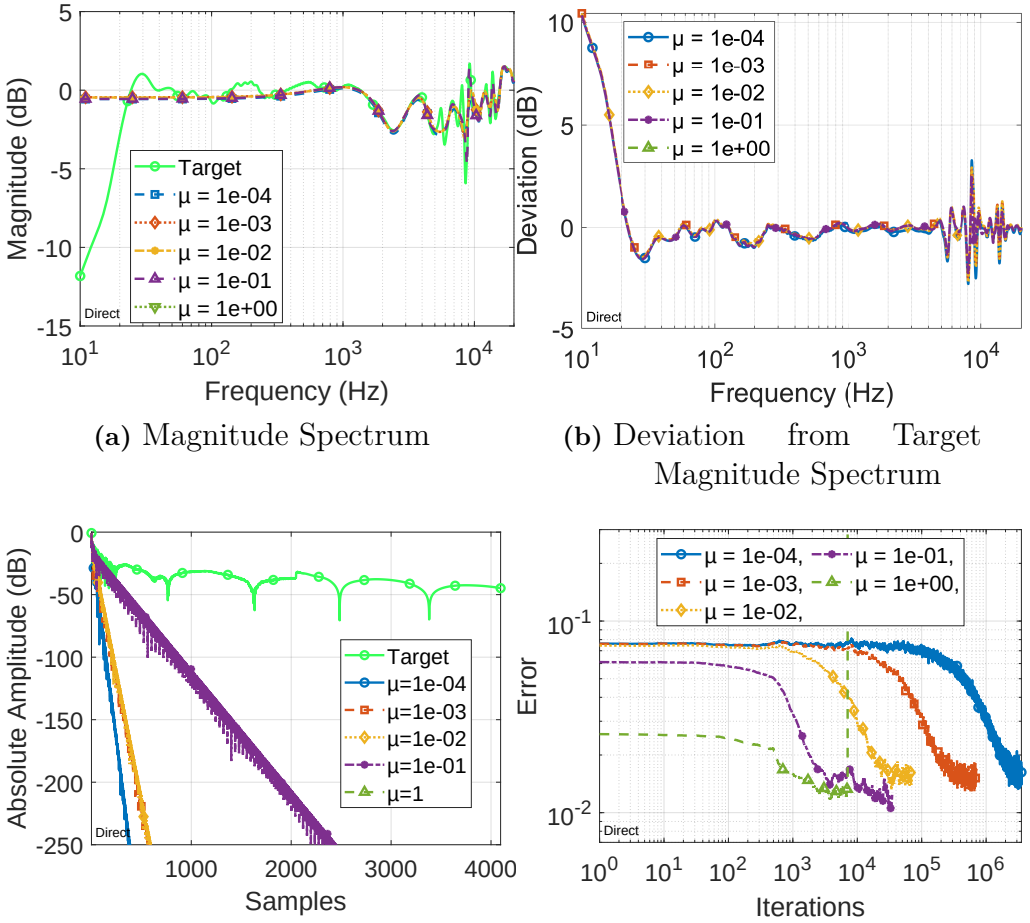

(a) Magnitude Spectrum

(b) Deviation from Target Magnitude Spectrum

(c) Absolute Impulse Response

(d) Output Error, $k = 1000$

Figure 4.1: Step-size Investigation, Estimating HpCFil, direct form filters, $M = 100$, $\mu \in [1 \times 10^{-4}, 1]$

In Figure 4.2 are the results of tests listed in 3.2 for estimation of a headphone compensation filter with a lattice form IIR filter representation.

Figure 4.2a shows the final magnitude response of the estimated filters and Figure 4.2b shows the deviation of the estimated filter magnitude response from the target magnitude response. Here, all filters that converged exhibit similar performance. The best performing step-size factor was $\mu = 0.1$ which better captured the sharp peaks and sub-peaks in the region approaching 10 kHz. One outlier in the magnitude response results was the case $\mu = 1$, where in the region f <100 Hz the filter achieved a high pass effect with a cutoff frequency around F =30 Hz.

Again Figure 4.2c shows the inverse relationship between step-size factor and rate of exponential decay of the filter. Here there is a periodic behaviour seen in the curve of $\mu = 0.1$, where a pattern of short sub-peaks repeat every 300-400 samples.

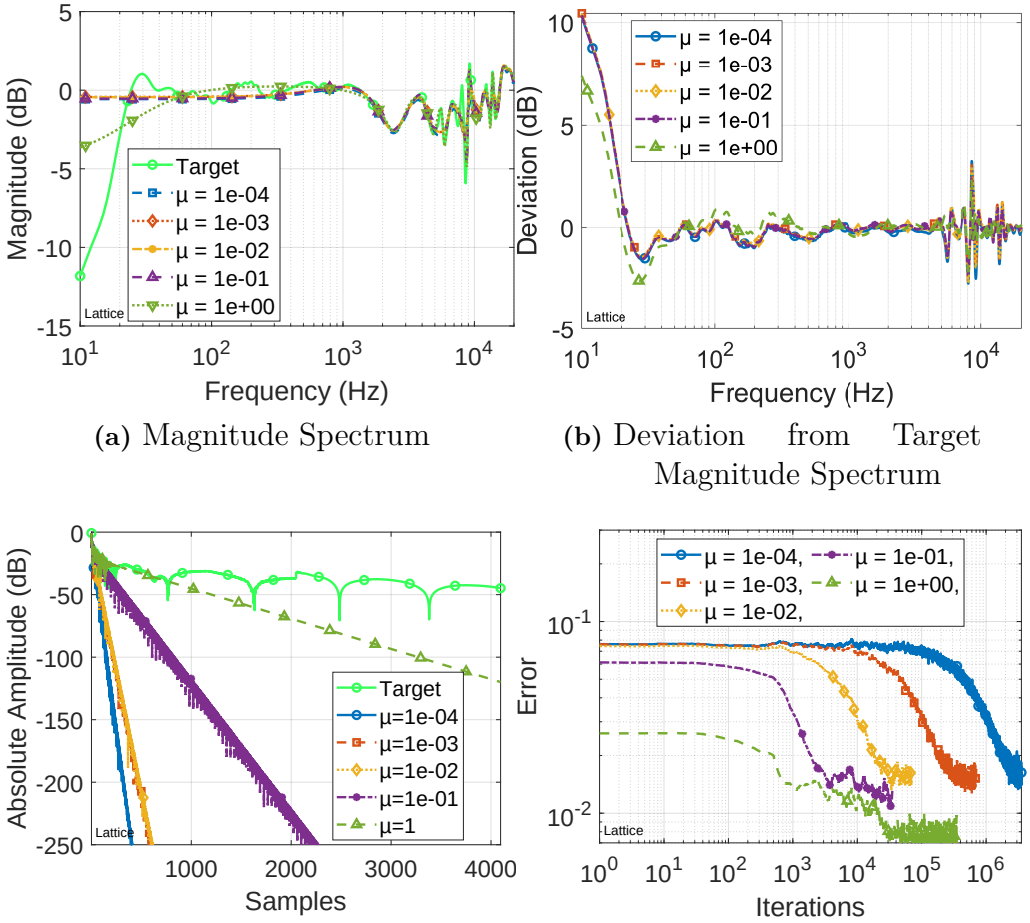

(a) Magnitude Spectrum

(b) Deviation from Target Magnitude Spectrum

(c) Absolute Impulse Response

(d) Output Error, $k = 1000$

Figure 4.2: Step-size Investigation, Estimating HpCFil, lattice form filters, $M = 100$, $\mu \in [1 \times 10^{-4}, 1]$

Figures 4.3 and 4.4 show the final estimated direct form filter coefficients for headphone compensation filter, in direct form, for direct form and lattice form filters. In the case of lattice form the coefficients were converted to direct form via Schur recursion in Algorithm 2.2. In the direct form case figure 4.3, for $\mu = 1$ the result diverged and no coefficients were found. In the cases for other step-size values the produced coefficients are similar.

In the lattice form estimations Figures 4.4a and 4.4b the largest step-size factor produced generally large and more varying coefficient values.

For 'b' coefficients, in Figures 4.3a and 4.4a, the estimations are generally close to the FIR impulse response amplitudes but worsen as μ increases above $\mu > 1\times10^{-2}$.

For 'a' coefficients, in Figures 4.3b and 4.4b, the two largest step-size factor estimations $\mu = [1, 0.1]$ are generally larger in amplitude.

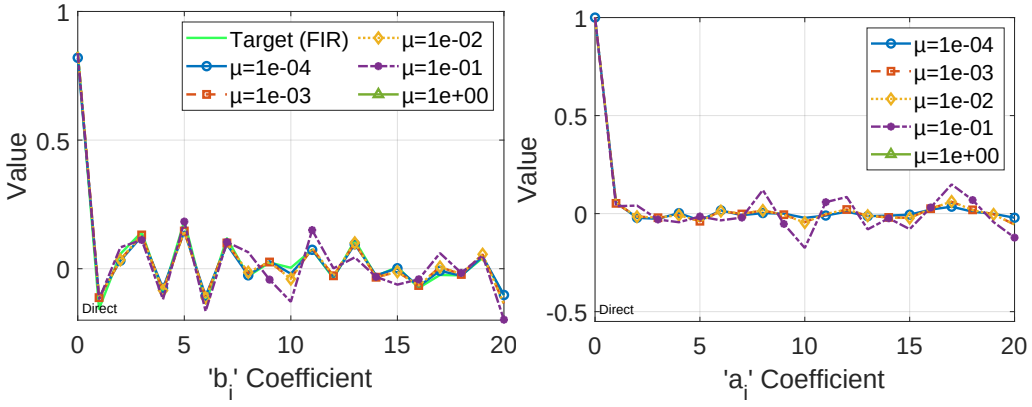

(a) b coefficient values, i is coefficient reference

(b) a coefficient values, i is coefficient reference

Figure 4.3: Filter coefficient values, Estimating Headphone Compensation Filter (Min Phase), Direct Form, $1 \times 10^{-4} \leq \mu \leq 1$

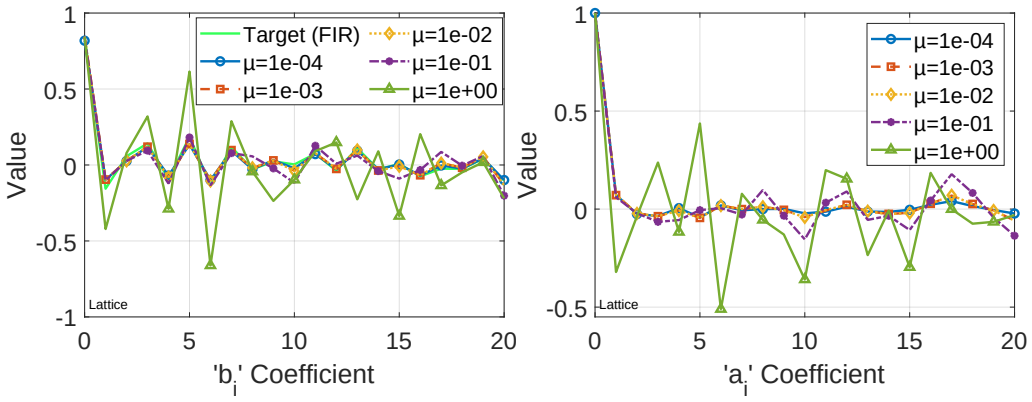

(a) b coefficient values, i is coefficient reference

(b) a coefficient values, i is coefficient reference

Figure 4.4: First 20 Filter Coefficients, Estimating Headphone Compensation Filter (Min Phase), Lattice Form, $1 \times 10^{-4} \leq \mu \leq 1$

4.1.2 HRTF Estimation

This section contains the results for the step-size investigation run using estimation of a HRTF. Figure 4.5 shows the performance indicators for the estimation with direct form filters and Figure 4.6 shows the same indicators for lattice form. In all subfigures, except Figures 4.5c and 4.6c, the differences are indistinguishable in this format, therefore a majority of observations from here on are made for both direct form and lattice form cases simultaneously.

The deviation from target magnitude response in Figures 4.5b,4.6b show an overall acceptable deviation of under 2 dB in all cases. In low frequencies $f < 400$ Hz the best case is again the largest step-size factor of $\mu = 1$. This is a similar anomaly as was observed in the estimation of the headphone compensation filter with lattice filter in Figure 4.2a, where the magnitude response was reduced in the region f <60 Hz.

Figures 4.5c and 4.6c show the decay in magnitude of the impulse responses. In both cases the gradient of the decays are similar and inversely proportional to the step-size factor, though with no observable relationship in this format. There is an observable difference in the magnitude of sub-peaks with smaller amplitudes for the direct form for all step-size factor values. As this is a magnitude representation of the impulse response, the significance of this may be little.

Figures 4.5d and 4.6d show the adaptive filter output error over iterations. Between $\mu = [1 \times 10^{-2}, 1 \times 10^{-3}, 1 \times 10^{-4}]$, for both filter forms the number of iterations to convergence is inversely affected by the step-size factor. Decreasing step-size factor by an order of magnitude increases the iterations to convergence by a similar order, additionally the final error is more variable upon convergence. Where $mu = [1 \times 10^{-1}, 1]$, this relationship is not present and the time to convergence is longer and the final error value is only marginally lower than the aforementioned results. Similar to what was seen in the corresponding results for the headphone compensation filter

Figures 4.1d and 4.2d, these step-size factors begin with a lower starting error value. However, for the HRIR estimations the direct form solution did converge in the case of $\mu = 1$.

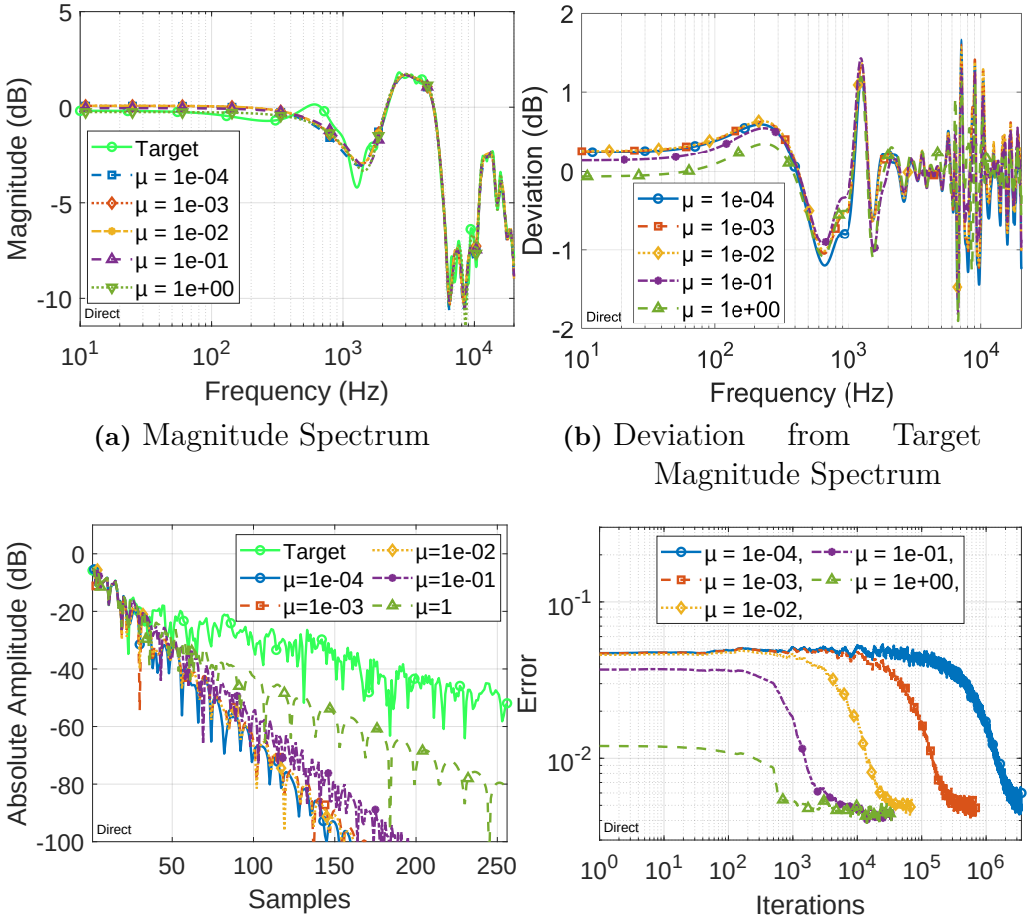

(a) Magnitude Spectrum

(b) Deviation from Target Magnitude Spectrum

(c) Absolute Impulse Response

(d) Output Error, $k = 1000$

Figure 4.5: Step-size Investigation, Estimating HRIR, direct form filters, $M = 20$, $\mu \in [1 \times 10^{-4}, 1]$

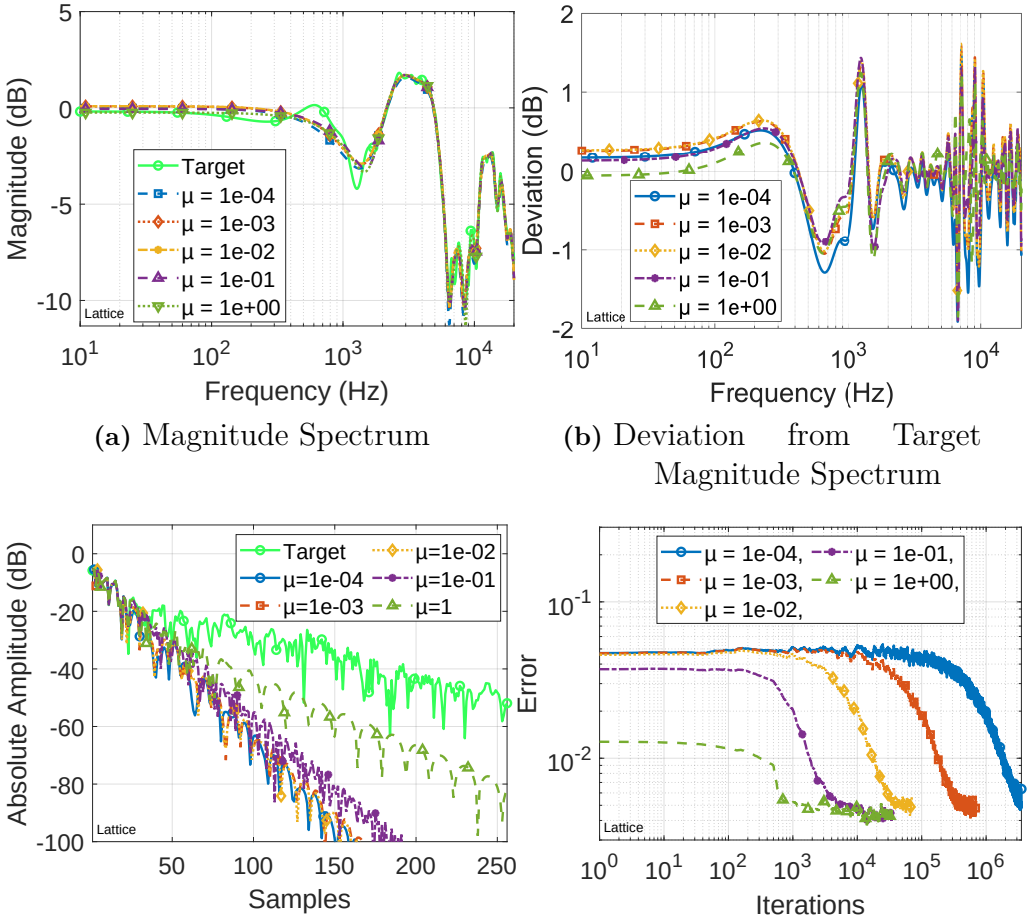

(a) Magnitude Spectrum

(b) Deviation from Target Magnitude Spectrum

(c) Absolute Impulse Response

(d) Output Error, $k = 1000$

Figure 4.6: Step-size Investigation, Estimating HRIR, lattice form filters, $M = 20$, $\mu \in [1 \times 10^{-4}, 1]$

Figures 4.7 and 4.8 show the final estimated direct form filter coefficients for an HRTF for direct form and lattice form filters. In the case of lattice form the coefficients were converted to direct form via Schur recursion in Algorithm 2.2. Both cases of direct form and lattice form are very similar.

For 'b' coefficients, in Figures 4.7a and 4.8a, the two largest step-size factor estimations are close to one another, and sometimes closer to the target, $i = 3, 9, 14, 15, 16, 17, 19$ at other coefficients they can be further off than the other estimations, $i = 8, 11, 12, 18$.

For 'a' coefficients, in Figures 4.7b and 4.8b, the two largest step-size factor estimations $\mu = [1, 0.1]$ are generally larger in magnitude.

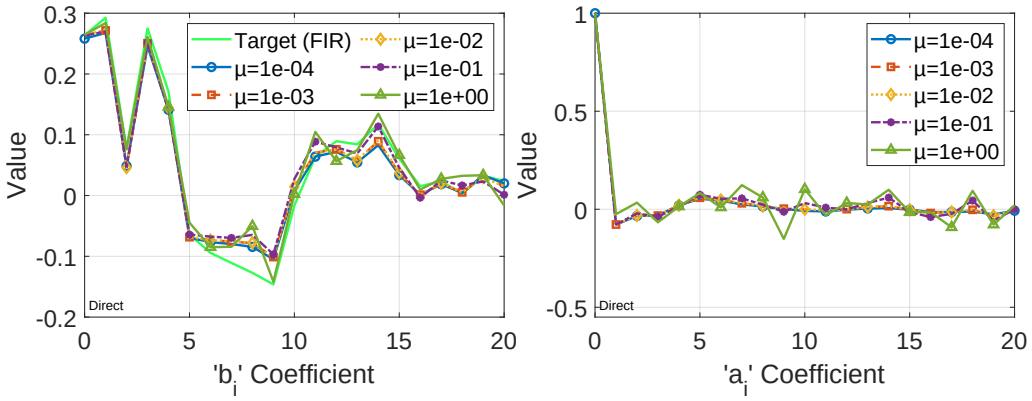

(a) b coefficient values, i is coefficient reference

(b) a coefficient values, i is coefficient reference

Figure 4.7: Filter coefficient values, Estimating HRIR (Min Phase), Direct Form, $1 \times 10^{-4} \leq \mu \leq 1$

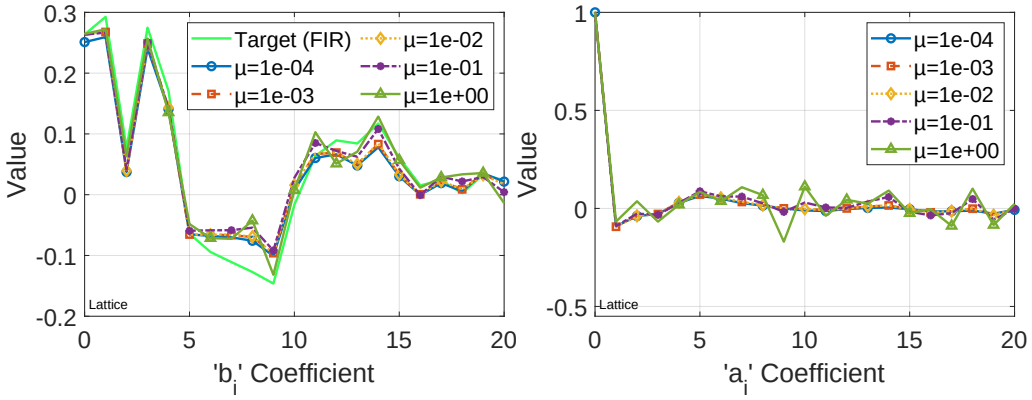

(a) b coefficient values, i is coefficient reference

(b) a coefficient values, i is coefficient reference

Figure 4.8: Filter Coefficients, Estimating HRIR (Min Phase), Lattice Form, $1 \times 10^{-4} \leq \mu \leq 1$

4.2 Minimum Order Investigation

The results for the minimum order investigations are presented below. This is separated into two subsection covering estimations of the headphone compensation filter in Section 4.2.1 and estimations of contralateral HRIR in Section 4.2.2.

4.2.1 Headphone Compensation Filter Estimation

Before proceeding with the estimation it is interesting to see the result of simply shortening the impulse response of the FIR filter that is being estimated. This will later provide a baseline upon which to assess any performance improvements made by modelling with a reduced order IIR filter.

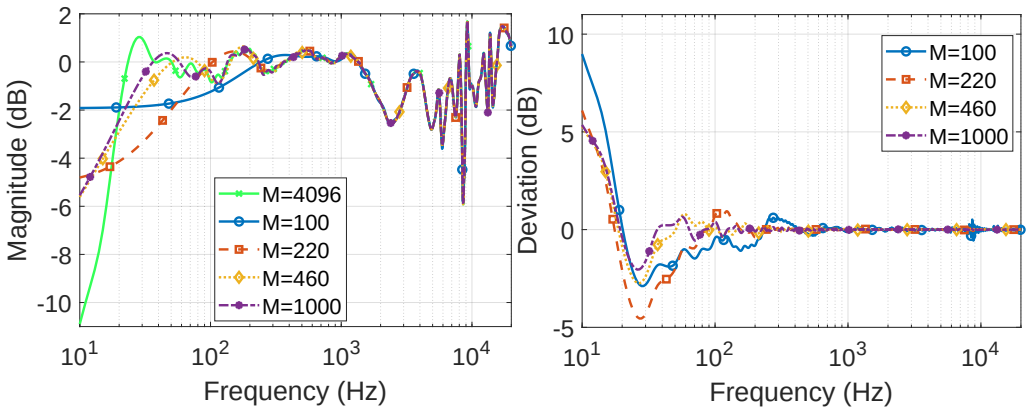

(a) Magnitude Spectrum

(b) Deviation from Full IR Magnitude Spectrum

Figure 4.9: Cut Impulse Response HpCFil (Min Phase) $100 \leq M \leq 1000$

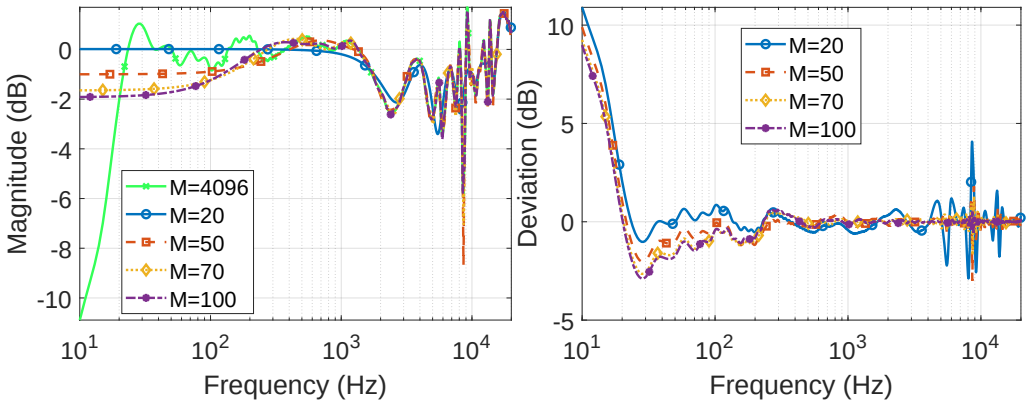

(a) Magnitude Spectrum

(b) Deviation from Full IR Magnitude Spectrum

Figure 4.10: Cut Impulse Response HpCFil (Min Phase) with IIR Direct Form $20 \leq M \leq 100$

The results of the high range minimum order test for estimation of headphone compensation filter are shown in for direct form in Figure 4.11 and lattice form in Figure 4.12. The results of the estimations using of direct form and lattice are indistinguishable from one another so presented results are combined here.

First the order error in Figures 4.11e and 4.12e show that all estimations converged with an approximately inverse linear relationship between filter order and convergence error value.

Observing the magnitude spectra in Figures 4.11a and 4.12a, the best performing is the highest order where $M = 1000$. Here it is seen that reducing order, increases the frequency at which the filter produces a more accurate estimation. This is shown also in Figures 4.11b and 4.12b, where one observes larger deviations from the target at higher frequencies for lower order filters. The filter performance is not necessarily worse over the whole frequency range for a lower order filter, in some positions it may by chance fit the filter curve more appropriately, however this is dependent on the target filter curve.

Figures 4.11d and 4.12d show the magnitude of the impulse response of the target and estimated filters. Interestingly, increasing the filter order has a similar effect to increasing the step-size in that the gradient of decay of the impulse response is reduced. Also, for $M = 1000$ the 'shape' of the absolute impulse response is now similar though skewed, sub-peaks occur sooner and the magnitude of peak amplitude begins to decay and diverge from the target.

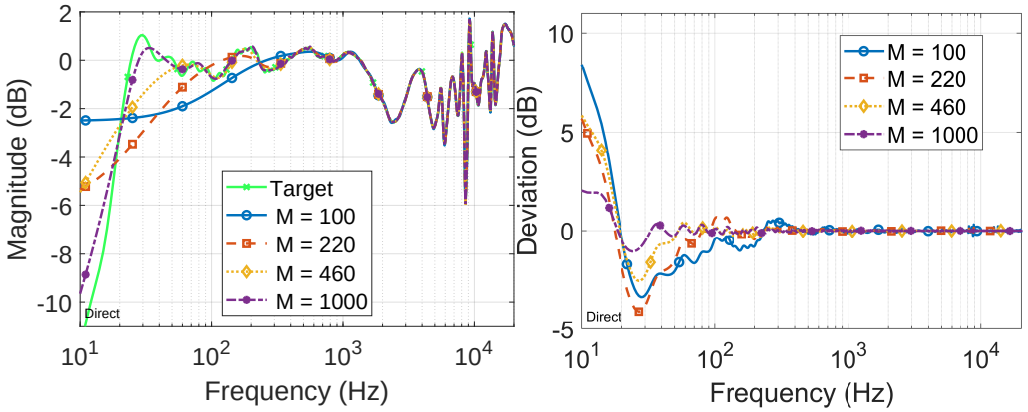

(a) Magnitude Spectrum

(b) Deviation from Target Magnitude Spectrum

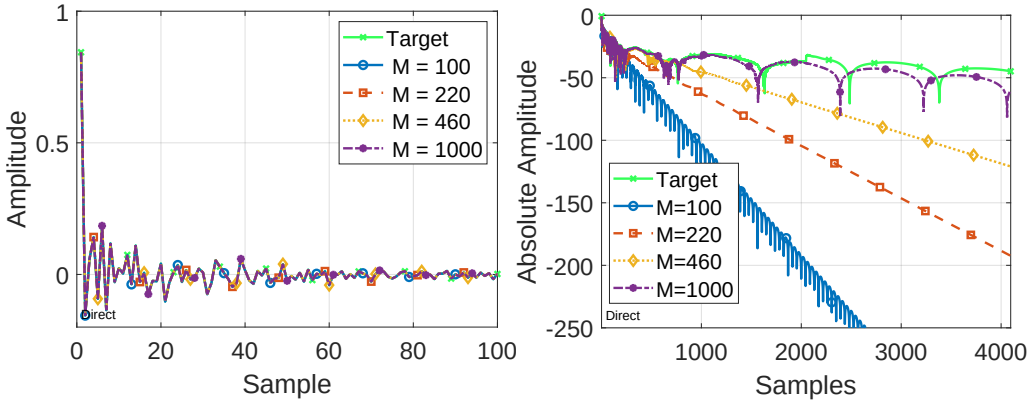

(c) Impulse Response Peak

(d) Absolute Impulse Response

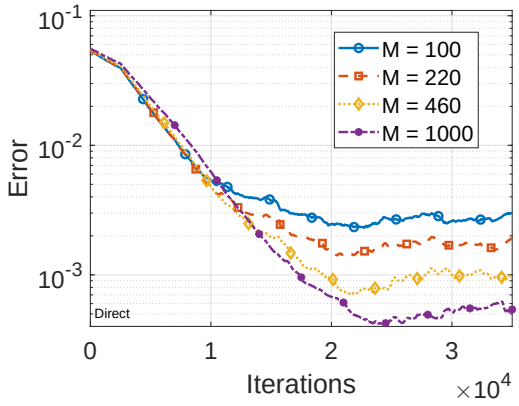

(e) Output Error, $k = 5000$

Figure 4.11: Order Investigation, Estimating HpCFil (Min Phase) with IIR Direct Form $100 \leq M \leq 1000$

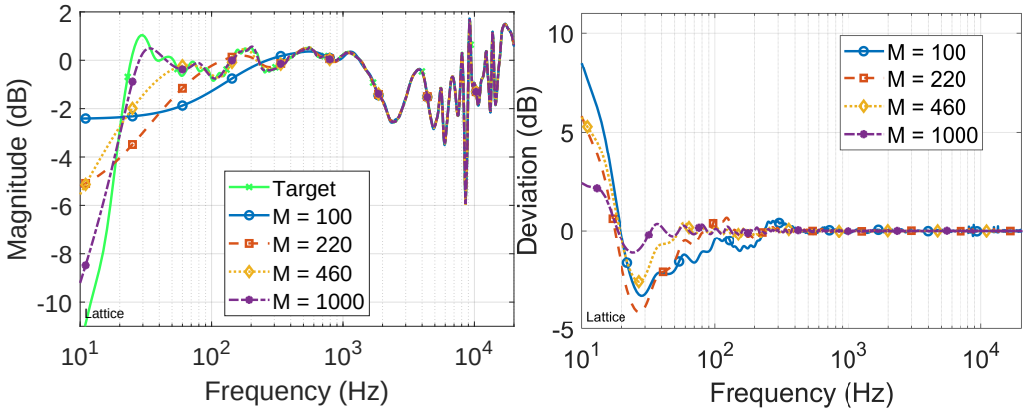

(a) Magnitude Spectrum

(b) Deviation from Target Magnitude Spectrum

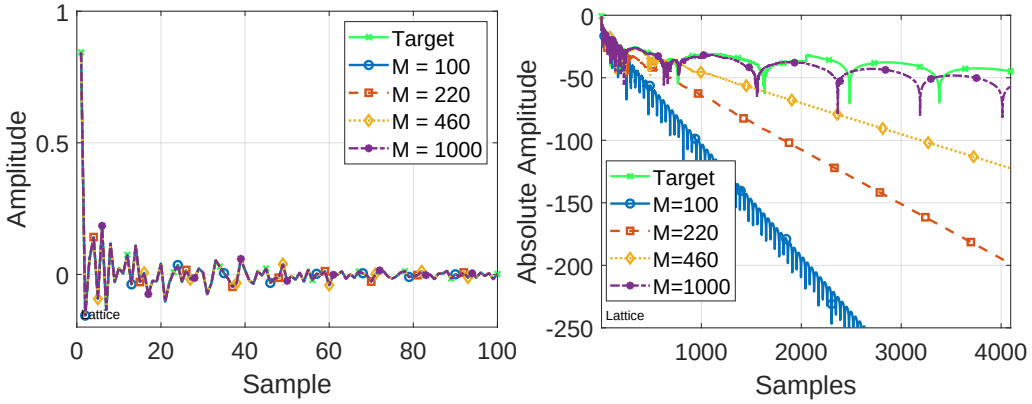

(c) Impulse Response Peak

(d) Absolute Impulse Response

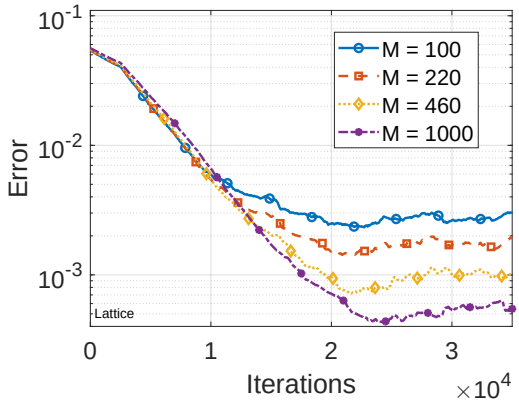

(e) Output Error, $k = 5000$

Figure 4.12: Order Investigation, Estimating HpCFil (Min Phase) with Lattice Form IIR $100 \leq M \leq 1000$

The results for the test in the very low filter order range, for direct from shown in Figure 4.13 and for lattice form shown in 4.14. Again here the results are quite similar between the two filter forms however some difference is seen across the filter orders, this is mostly visible in Figures 4.13d and 4.14d which will be discussed later.

Starting again with the order error convergence shown in Figures 4.13e and 4.14e, here the relationship between order error at convergence and filter order is also an approximately linear relationship, as much as was seen in the high range case in Figures 4.11e and 4.12e.

The filter performance in frequency domain is shown in Figures 4.13a and 4.14a. Here the accuracy of the filters is closely matched, with a minor difference in accuracy above 1000 Hz. In the low frequency range the increasing filter order results in a greater attenuation after the roll-off of the high-pass like feature. Here some difference is seen between the filter strucutres with direct form reaching $-2.5\,\mathrm{dB}$ and lattice form $-3.5\,\mathrm{dB}$ at 10 kHz. Figures 4.13b and 4.14b show that the larger order filter does have worse predictions in lower frequency ranges where the smooth curve of the estimated filter deviates further form the target filter curve. In he high frequency range above 4 kHz the $M = 20$ filter estimation degrades. In this region there are many sharp peaks and sub-peaks which are difficult to resolve with low filter orders.

Figures 4.13d and 4.14d show some of the minor differences between the direct form and lattice form estimation at low orders. In the direct form case Figure 4.13d the magnitude of impulse responses decays for $M = 50$ and $M = 70$ are very close, whereas in the lattice case Figure 4.14d they behave as was seen previously where the larger filter order has a lower decay gradient. In the case where $M = 100$ the direct form displays a more noisy or varying magnitude of decay up to 500 samples, whereas this same effect is seen to extend to 1000 samples in length for the lattice form. Additionally the direct form results in a lower gradient of decay relative to the lattice form.

The results for the very large filter order in Figure 4.15 show the order length required to achieve very small deviation from the target magnitude response. An unexpected result was that of the largest filter of order $M = 2300$ converged to a manifold in the error space as seen in 4.15e. This resulted in a very noisy impulse response, shown in Figure 4.15d and a relatively significant deviation in the peak and sub-peak around 9 kHz shown in the deviation in Figure 4.15b. The filter of order $M = 2000$ performs excellently, even beginning to capture the peak seen just above 2000 samples in the absolute impulse response in 4.15, which was not represented in the smaller filter orders $M = [1000, 1600]$.

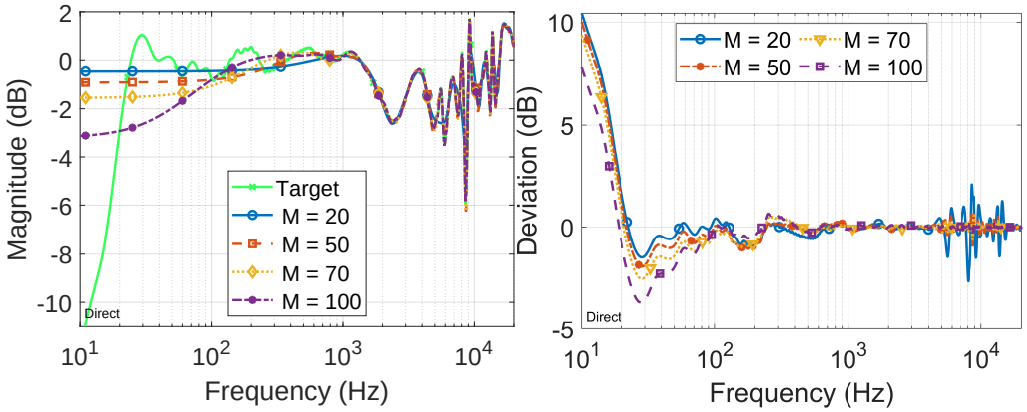

(a) Magnitude Spectrum

(b) Deviation from Target Magnitude Spectrum

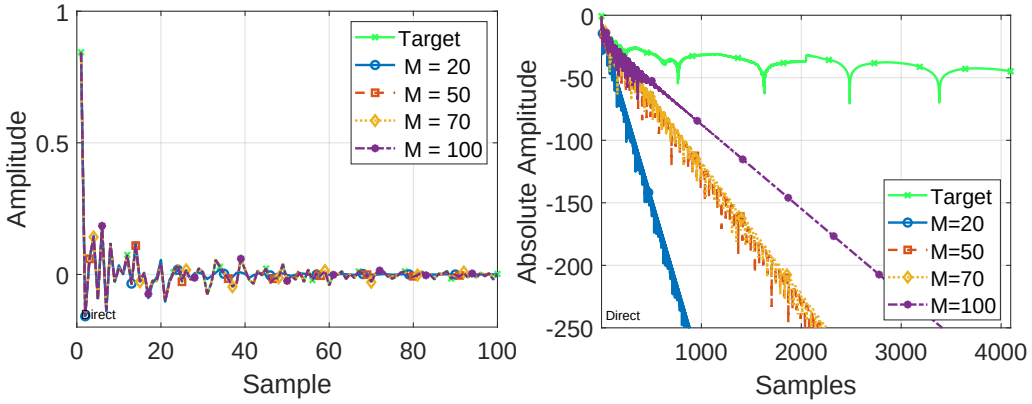

(c) Impulse Response Peak

(d) Absolute Impulse Response

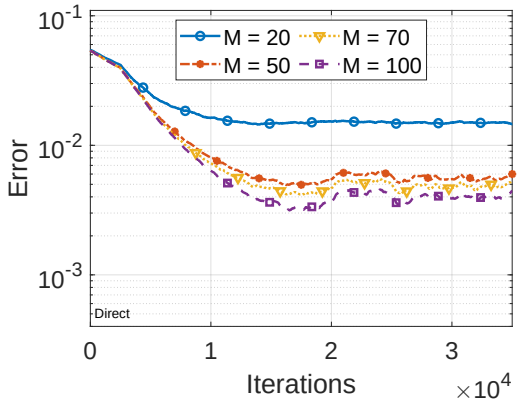

(e) Output Error, $k = 5000$

Figure 4.13: Order Investigation, Estimating HpCFil (Min Phase) with Direct Form IIR $20 \leq M \leq 100$

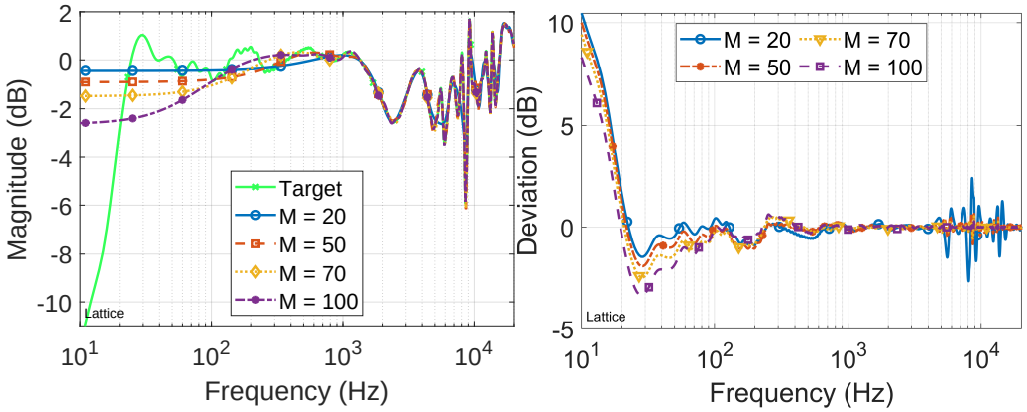

(a) Magnitude Spectrum

(b) Deviation from Target Magnitude Spectrum

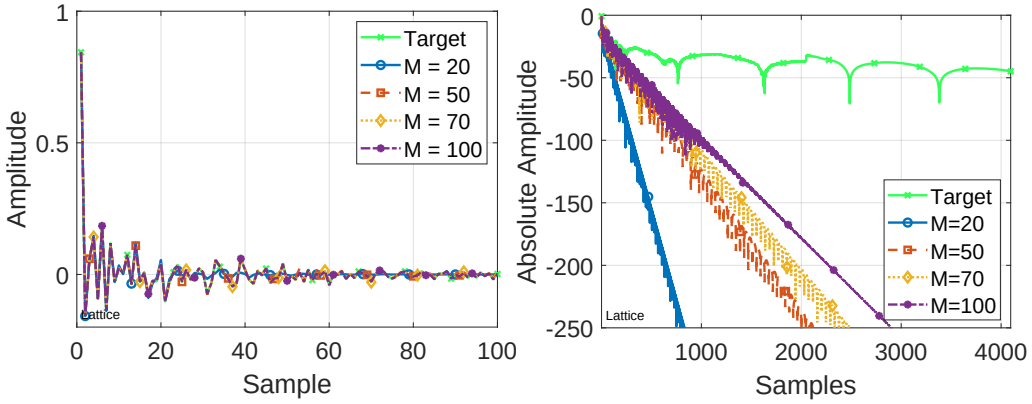

(c) Impulse Response Peak

(d) Absolute Impulse Response

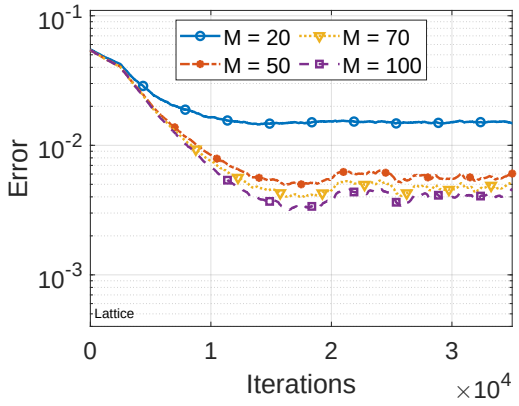

(e) Output Error, $k = 5000$

Figure 4.14: Order Investigation, Estimating HpCFil (Min Phase) with Lattice Form IIR $20 \leq M \leq 100$

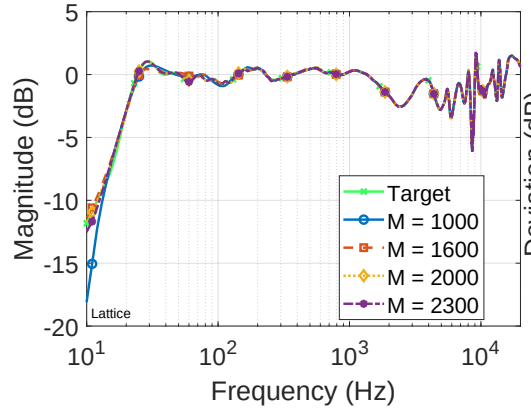

(a) Magnitude Spectrum

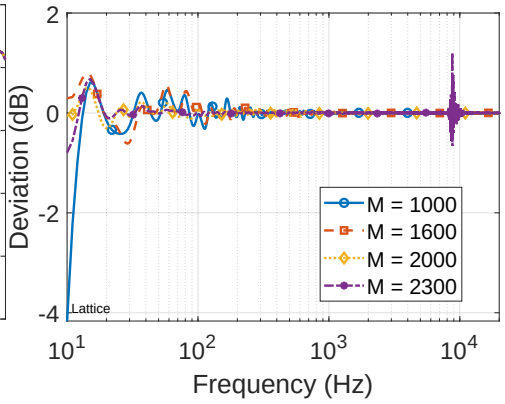

(b) Deviation from Target Magnitude Spectrum

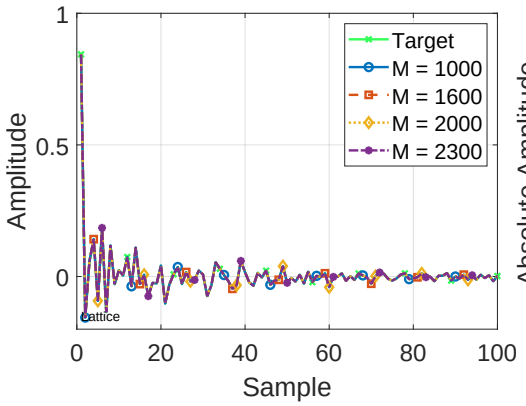

(c) Impulse Response Peak

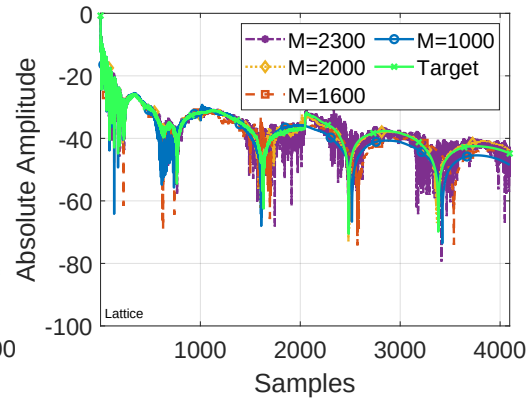

(d) Absolute Impulse Response

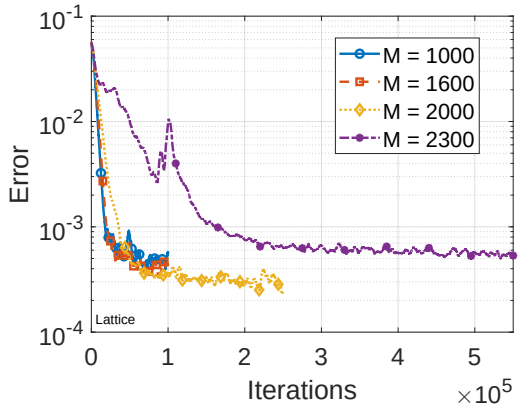

(e) Output Error, $k = 5000$

Figure 4.15: Order Investigation, Estimating HpCFil (Min Phase) with Lattice Form IIR $1000 \leq M \leq 2300$

Figure 4.16 shows, for four filter orders, the resulting magnitude spectra for both a cut FIR impulse response and estimation of the system with an adaptive lattice form IIR filter. In the low filter order case in Figure 4.16a for the solution $M = 20$ improvements in the region 4 kHz-15 kHz where sharp peaks are more closely

represented relative to the cut FIR. Additionally better performance is seen around the 1 kHz and 1.5 kHz peak and sub peak respectively. Both filters exhibit a flat response in the low frequency region and fail to capture the high-pass roll-off in the 10 Hz-30 Hz region. For filter order $M = 100$, performance is similar between the two but again with the IIR filter better capturing the Sharp peaks at 9 kHz. Both filters again fail to capture the high-pass roll-off in the 10 Hz-30 Hz region.

In the high filter order case in Figure 4.16c the performance in the high frequency is indiscernible above 300 Hz for $M = 220$ and above 200 Hz for $M = 1000$. The differences below these points for the $M = 220$ case are not significant but the IIR filter achieves a steeper roll-off. For the $M = 1000$ case the IIR filter achieves a significantly better performance than the FIR case, the peak at 28 Hz and high-pass roll-off are much more closely represented by the IIR filter.

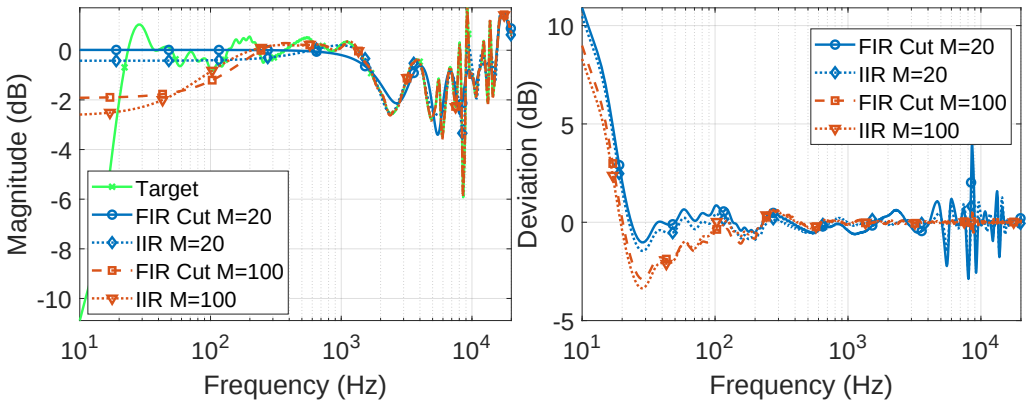

(a) Magnitude Spectrum $M = 20, M = 100$

(b) Deviation from Target $M = 20, M = 100$

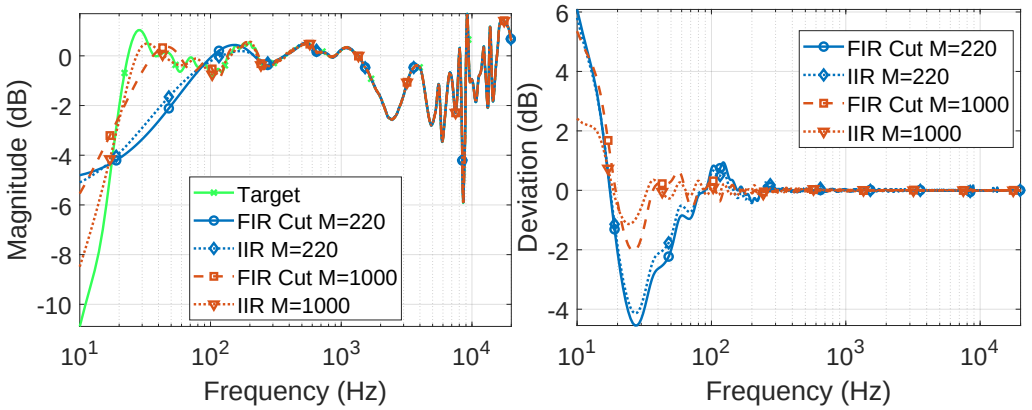

(c) Magnitude Spectrum $M = 220, M = 1000$

(d) Deviation from Target $M = 220, M = 1000$

Figure 4.16: Comparison of Cut FIR and IIR estimations of Headphone compensation filter using lattice form filter, low and high order

4.2.2 HRIR Estimation

Again for this system the effect on the magnitude response when cutting the FIR filter impulse response is plotted in Figures 4.17 and 4.18. This provides a baseline to compare the performance of the IIR estimations.

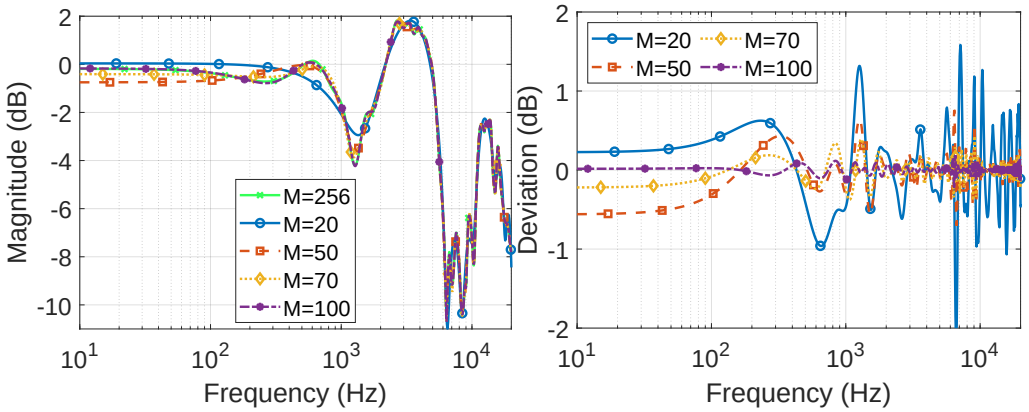

(a) Magnitude Spectrum

(b) Deviation from Full IR Magnitude Spectrum

Figure 4.17: Cut Impulse Response HRIR (Min Phase) $20 \leq M \leq 100$

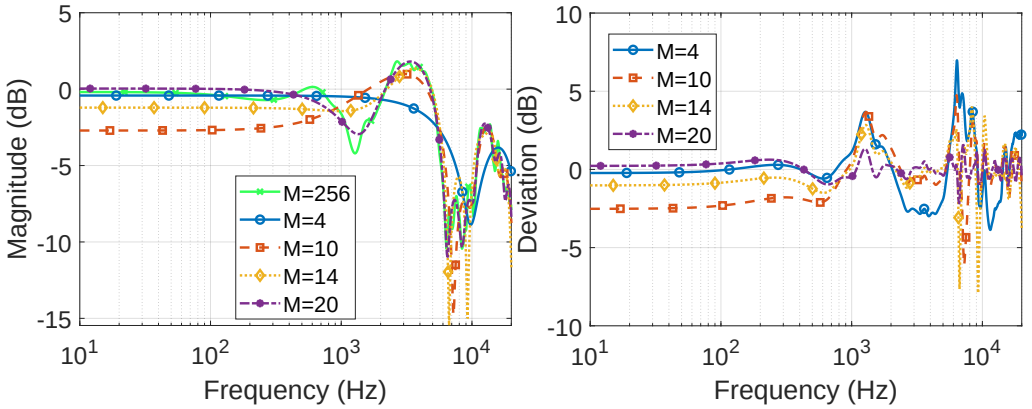

(a) Magnitude Spectrum

(b) Deviation from Full IR Magnitude Spectrum

Figure 4.18: Cut Impulse Response HRIR (Min Phase) $4 \leq M \leq 20$

The results from the high range of filter orders for both direct and lattice form filter structures are shown in Figures 4.19 and 4.20. As with other high order cases there is little difference observable in the produced filters, in frequency domain. Figures 4.19b and 4.20b show that all filter orders except $M = 20$ results in less than 1 dB. Figures 4.19a and 4.20a show where that the estimated filters show good estimation yet with a reducing filter order comes an impeded ability to capture fine details and sharp peaks in the upper frequency range. For example the feature around 3000 Hz,

is resolved by the $M = [70, 100]$ but not by $M = [20, 50]$ filters and the depth of the sub-peak at 1200 Hz is only well estimated by the $M = 100$ filter with reducing accuracy as filter order decreases.

Figures 4.19d and 4.20d show the previously observed effect of filter order on the magnitude of the impulse response, whereby, after the length of the filter order, the rate of decay of the impulse response is increased by reducing the filter order.

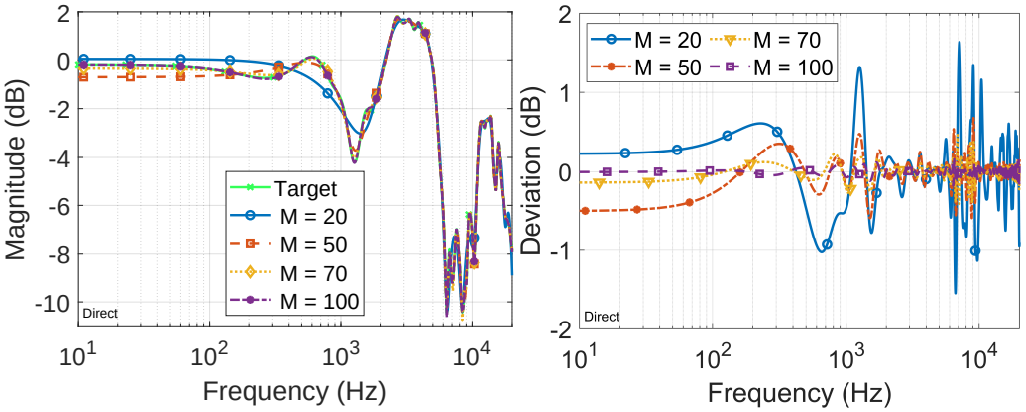

(a) Magnitude Spectrum

(b) Deviation from Target Magnitude Spectrum

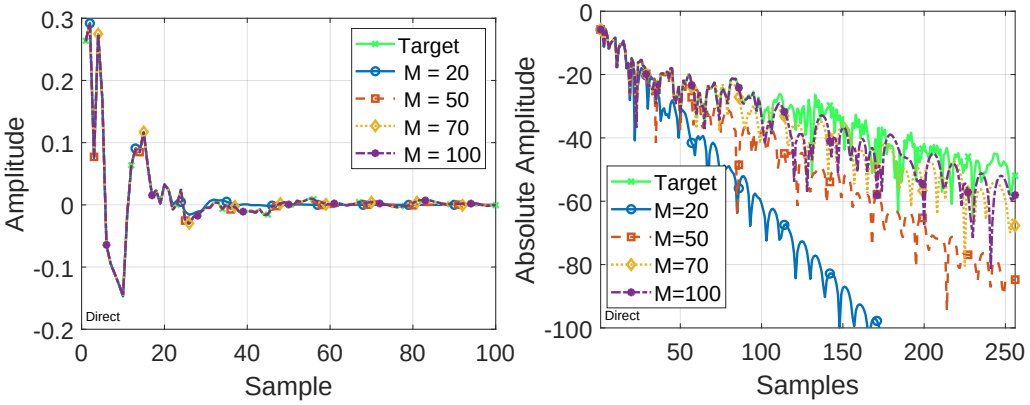

(c) Impulse Response Peak

(d) Absolute Impulse Response

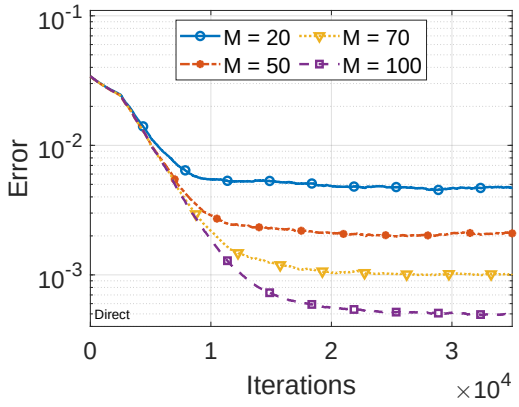

(e) Output Error, $k = 5000$

Figure 4.19: Order Investigation, Estimating HRIR (Min Phase) with Direct Form IIR, $20 \leq M \leq 100$

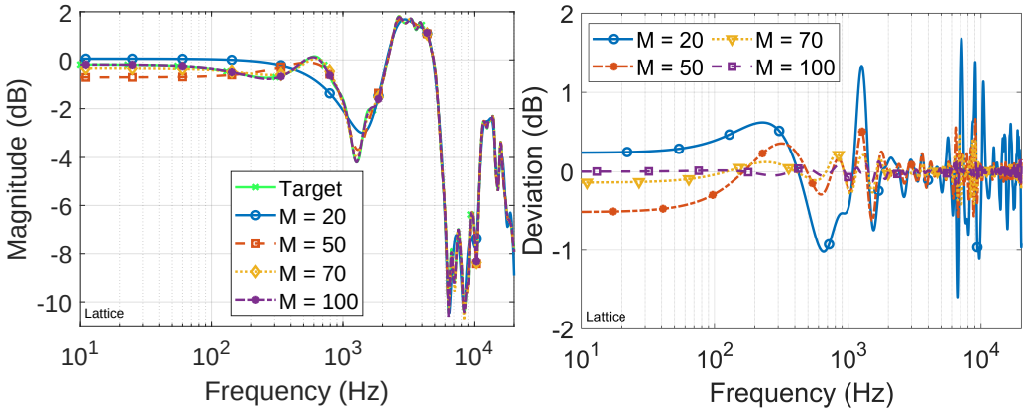

(a) Magnitude Spectrum

(b) Deviation from Target Magnitude Spectrum

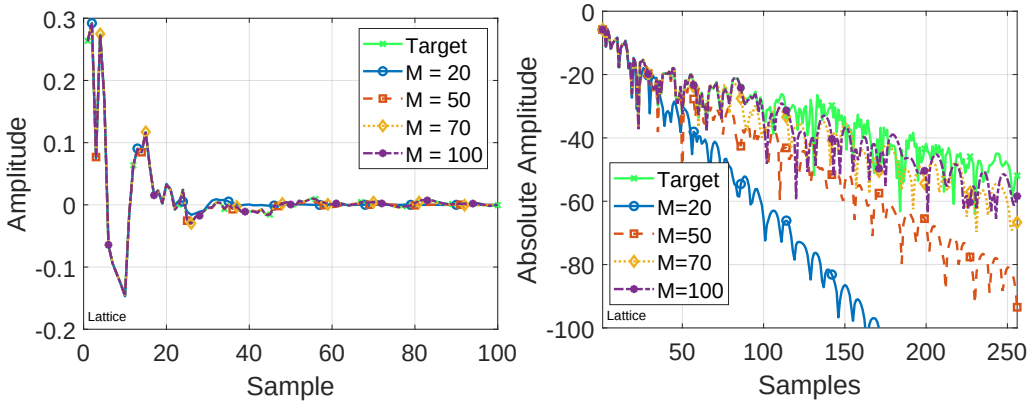

(c) Impulse Response Peak

(d) Absolute Impulse Response

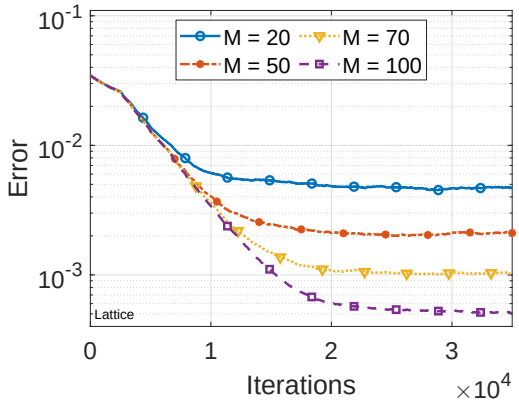

(e) Output Error, $k = 5000$

Figure 4.20: Order Investigation, Estimating HRIR (Min Phase) with Lattice Form IIR $20 \leq M \leq 100$

The results of the low filter order range estimations of head related transfer functions for both direct form and lattice form filter are shown in Figures 4.21 and 4.22.

Observing the magnitude spectra in Figures 4.21a and 4.22a shows that increasing filter order improves the filter's ability to resolve finer details and sharper changes in the curve across the frequency spectrum. An unexpected result of this is the case of $M = 10$ which manages to match the height of the peak around 3 kHz but the roll-off then results in a filter with a flat response but at -2 dB instead of near zero.

In figures 4.21c and 4.22c the effect of the filter order is seen clearly in the peak region where the filters are able to accurately model the desired impulse response up to the length of the zero coefficients, after which some energy is maintained by the feedback or pole coefficients but is not able to accurately model the response.

What occurs later in the Impulse response is better shown by Figures 4.21d and 4.22d where the magnitude of the impulse response is defined by some rate of decay that is inversely related to the filter order.

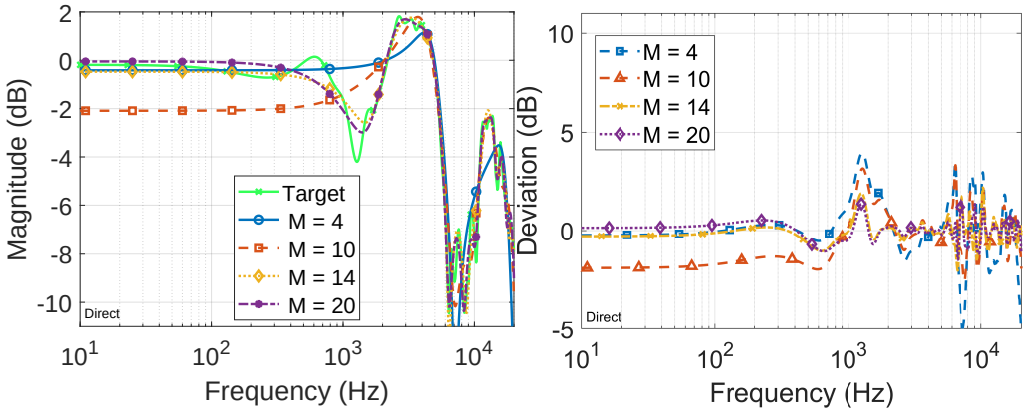

(a) Magnitude Spectrum

(b) Deviation from Target Magnitude Spectrum

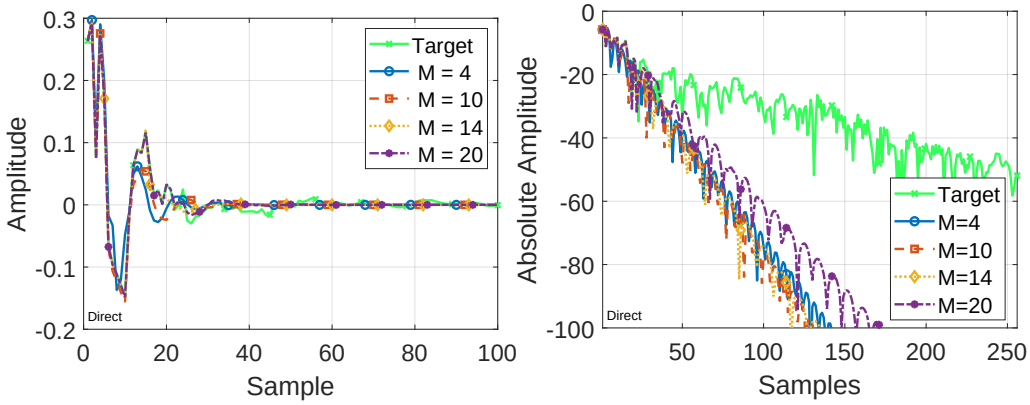

(c) Impulse Response Peak

(d) Absolute Impulse Response

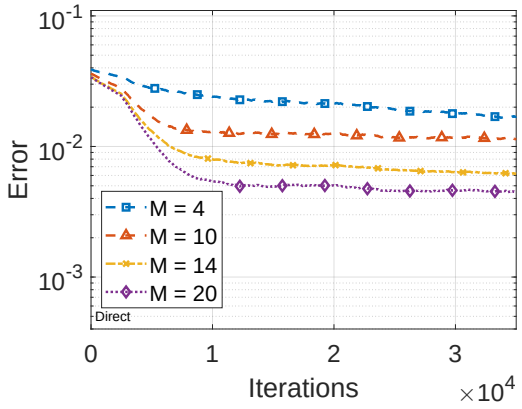

(e) Output Error, $k = 5000$

Figure 4.21: Order Investigation, Estimating HRIR (Min Phase) with Direct Form IIR, $1 \leq M \leq 20$

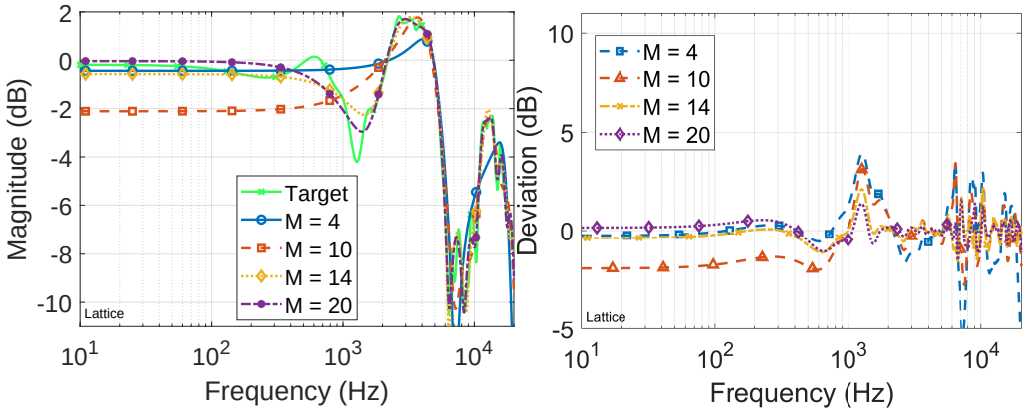

(a) Magnitude Spectrum

(b) Deviation from Target Magnitude Spectrum

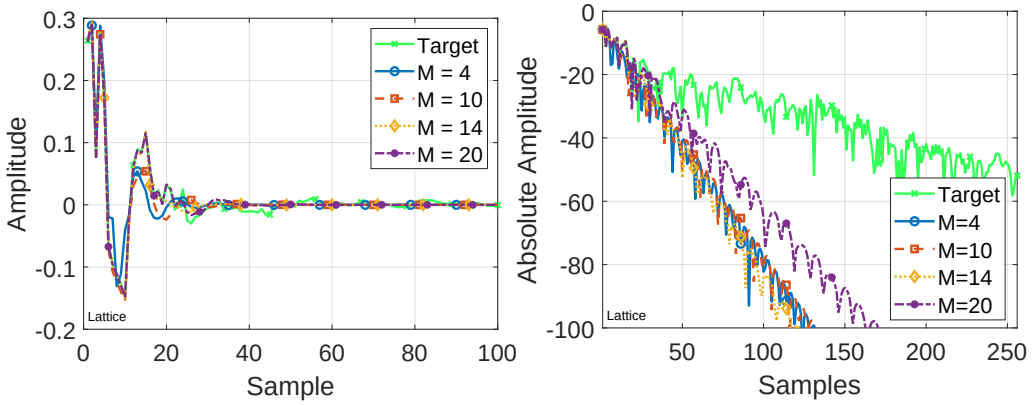

(c) Impulse Response Peak

(d) Absolute Impulse Response

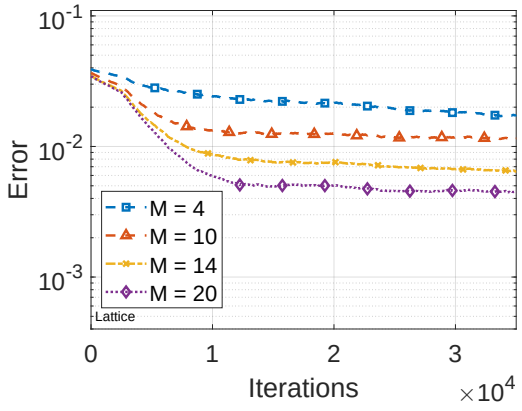

(e) Output Error, $k = 5000$

Figure 4.22: Order Investigation, Estimating HRIR (Min Phase) Lattice Form IIR, $1 \leq M \leq 20$

Figure 4.23 shows, for four filter orders, the resulting magnitude spectra for both a cut FIR impulse response and estimation of the system with an adaptive IIR filter. In the low filter order case in Figure 4.23a there is some improvement on filter performance by the IIR filter relative to the cut FIR. In the case $M = 4$ this is

especially evident in the peaks around 3 kHz-4 kHz, though the improvement is not significant. Similarly in the $M = 20$ case this peak is also better captured as well as the sub-peak at 7 kHz where the FIR filter overshoots.

In the high filter order case in Figure 4.23c there is no discernible difference between the cur FIR filter and the IIR filter estimation, any improvements are relatively small in the sharp peaks found between 6 kHz-10 kHz.

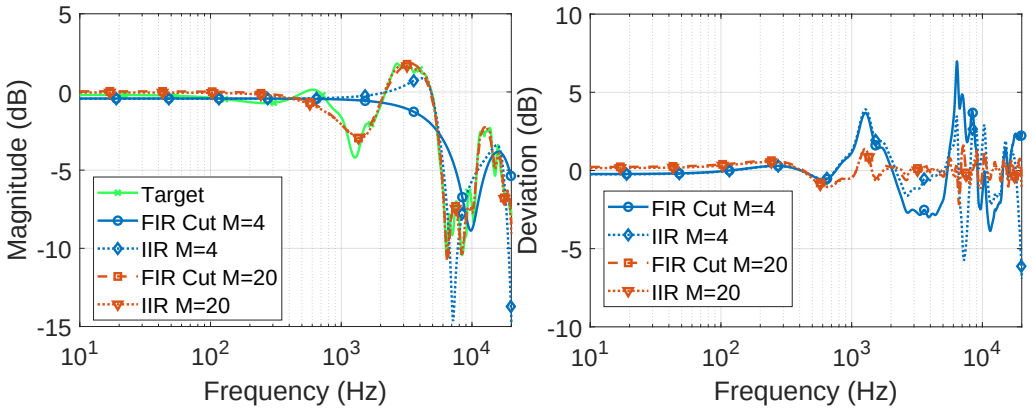

(a) Magnitude Spectrum $M = 4, M = 20$

(b) Deviation from Target $M = 4, M = 20$

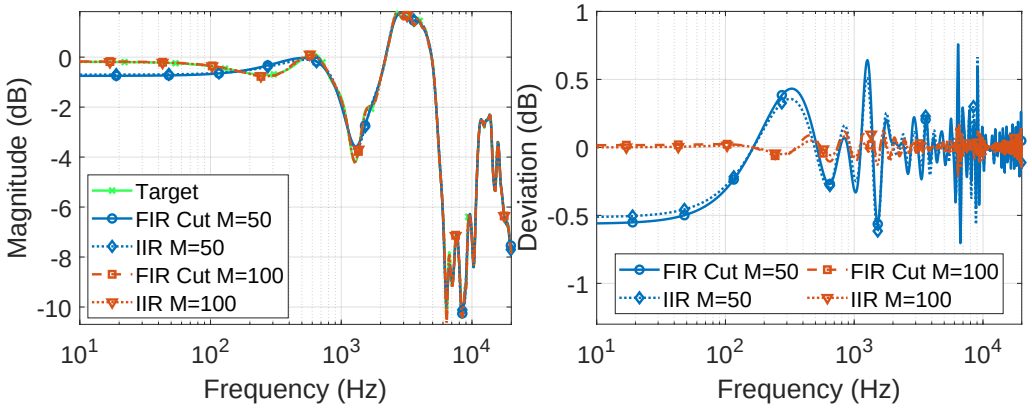

(c) Magnitude Spectrum $M = 50, M = 100$

(d) Deviation from Target $M = 50, M = 100$

Figure 4.23: Comparison of Cut FIR and IIR estimations of HRIR using lattice form filter, low and high order

Looking at the results for the binaural channel estimations with an IIR lattice filter of order of $M = 150$ in Figure 4.24 there are some discrepancies in the accuracy of the estimation. The magnitude response in Figure 4.24a shows a large unexpected peak at 6 kHz, also the response deviates visibly in the region below 700 Hz. Observing the deviation shows that the contralateral estimation has much smaller deviation from the target than the ipsilateral estimation. The magnitude of impulse response in Figure 4.24d reveals that the ipsilateral case exhibits a less uniform decay rates across the impulse response with three decays separated by flat regions. The Figure

4.24e confirms that the filters reached a converged result.

Interestingly when comparing the binaural channel estimations with IIR lattice filter of order of $M = 50$ in Figure 4.25 the performance is improved slightly for the ipsilateral channel. In Figure 4.25e the order error, relative to $M = 150$, is reduced slightly for the ipsilateral channel and increased by an order of magnitude for the contralateral channel. In Figure 4.25b the large peak seen in $M = 150$ is reduced with the largest deviation peakof $+-1.5\,\mathrm{dB}$ now at $8\,\mathrm{kHz}$. Deviation across the rest of of the spectrum are increased in magnitude for both channels. Figure 4.25d shows how both channel decays are now below the target amplitude decay rates.

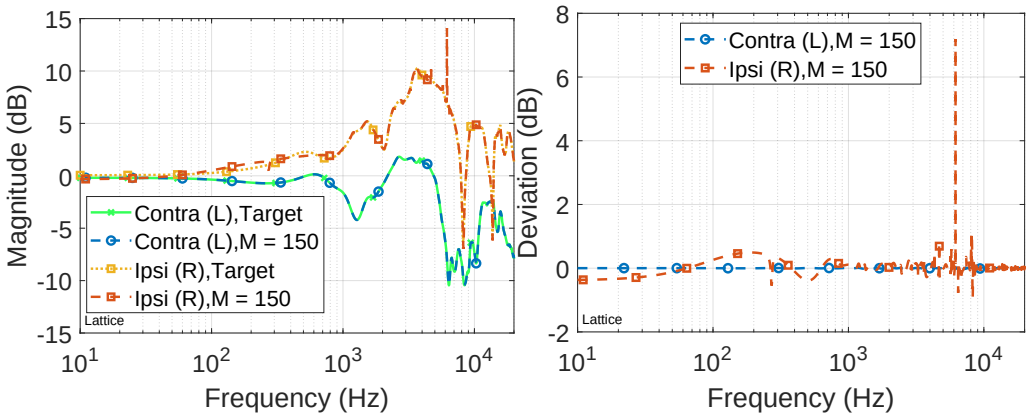

(a) Magnitude Spectrum

(b) Deviation from Target Magnitude Spectrum

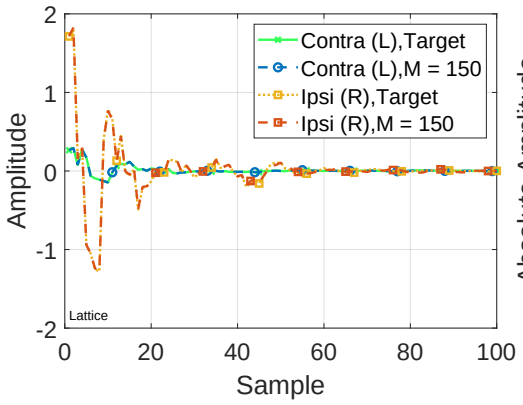

(c) Impulse Response Peak

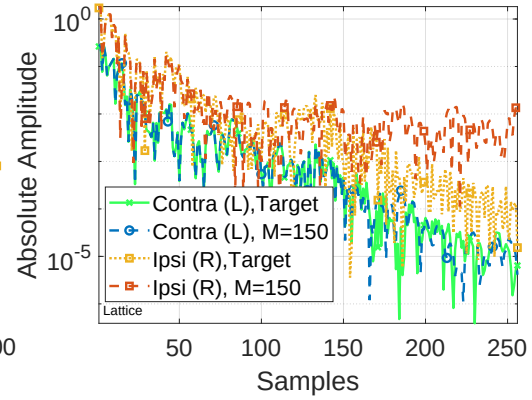

(d) Absolute Impulse Response

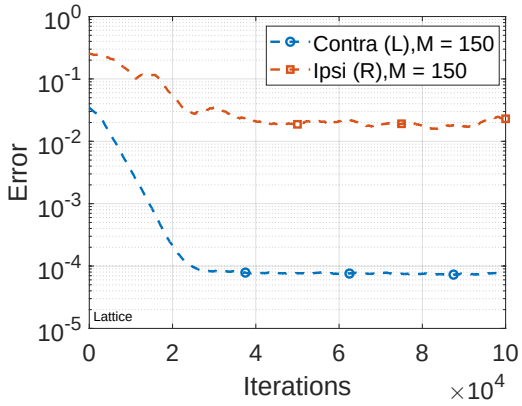

(e) Output Error, $k = 5000$

Figure 4.24: HRTF binaural estimation comparison, Lattice Form IIR, $M = 150$, N=1×10^5

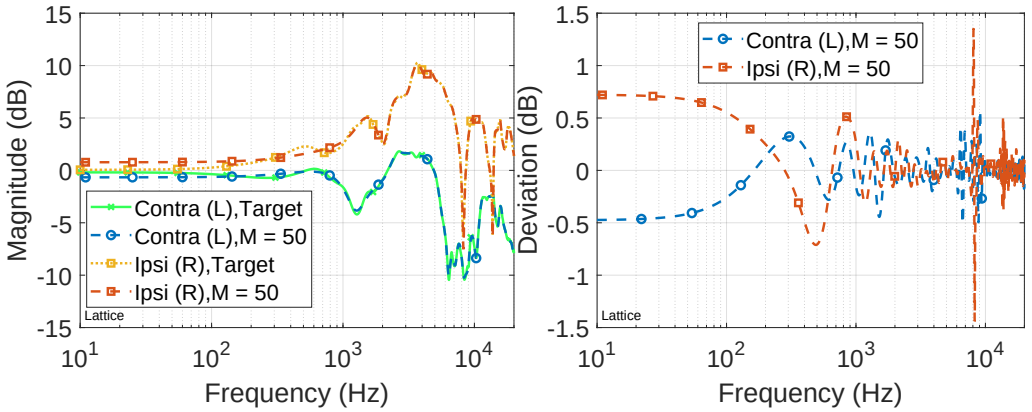

(a) Magnitude Spectrum

(b) Deviation from Target Magnitude Spectrum

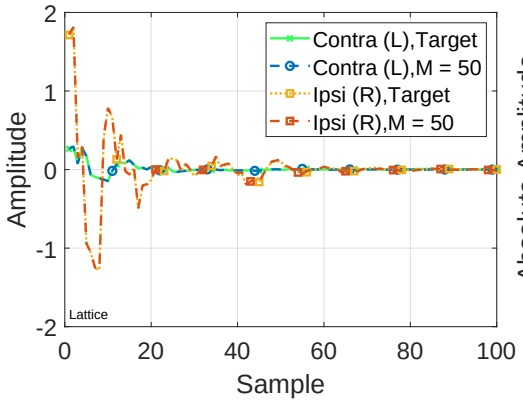

(c) Impulse Response Peak

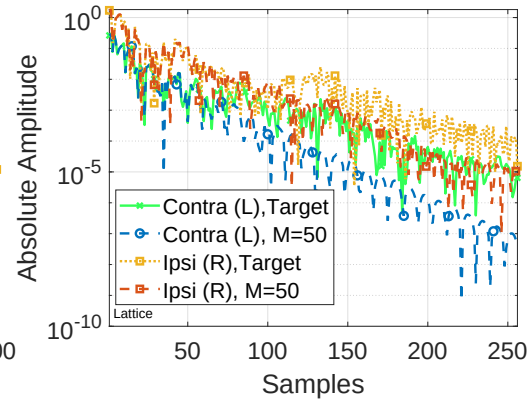

(d) Absolute Impulse Response

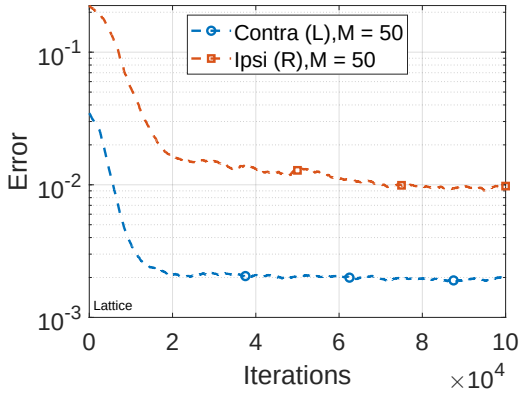

(e) Output Error, $k = 5000$

Figure 4.25: HRTF binaural estimation comparison, Lattice Form IIR, $M = 50$, N=1×10^5

5

Discussion

In this chapter the results will be discussed and explained with in the context of the theory and research questions. The significance of the results in relation to the specific applications will also be discussed.

5.1 Filter Structure Comparison

The algorithms implemented here are developments upon the simplest, gradient descent based, direct form and lattice form, time-domain adaptive filters. [1, Ch. 7] The key advantage of a lattice filter over a direct form filter is the stability test. This is evident in the step-size investigation when observing the output error convergence plots, where in the case of $M = 1$ the direct form in Figure 4.5d did not converge and the lattice form in Figure 4.5d did reach convergence. This was also the case in the very large filter estimations where only the lattice form filter of Figure 4.15 was able to converge in the highest filter order estimations. There are some very marginal differences in the decays of energy in the low order estimations of the headphone compensation filter, specifically $M = 70$ in Figures 4.13d and 4.14d. This was not consistent for all filter orders or observed in other cases so no conclusion is made about this result.

5.2 Step-size Investigation

The step-size factor modifies the size of the adjustment of coefficient values taken at each step. Therefore, the result of choosing a step-size factor of $\mu \to 0$ means a slower adaption.[6, Ch. 9] A step-size factor of $\mu < 1$ is required to maintain the assumption that the filter is time-invariant with sufficiently small changes each iteration step.[1, Ch. 7] More generally, when minimising a convex function with an iterative algorithm and a constant, non-vanishing step-size factor, the precise minimum is never reached which results in the error residual oscillating around the minimum point. Upon reaching convergence and as time tends to infinity, the mean of these converged values tends towards the optimal result. Therefore this oscillation can be seen as a variance of the mean converged value.[10, Ch. 14] As a result, choosing a smaller step-size coefficient will reduce this variance and potentially produce a more accurate result. The assumption made in this conclusion is that the target function is not undermodelled by the adaptive filter and that the global minimum is reached in each case.

When looking at the order error convergence results for all systems and filter structures in Figures 4.5d,4.6d,4.1d,4.2d, the output error on convergence is reduced with an increasing step size. This is contrary to the result predicted by the theory. One difference in this case is that the system in this experiment is undermodelled. This means that the filter is well modelled by the algorithm in the time domain up to the length of the filter order, after which the feedback coefficients create an infinitely decaying response. So, whilst the variance may be reduced and the accuracy improved within this sufficiently modelled region of length M, after this point the accuracy is dependent on the decay rate which in turn is dependent on the filter coefficient values.

In Figure 4.2, the effect of IIR decay on the estimation error in the lattice filter estimation of the headphone compensation filter seen. Figure 4.4 shows increased magnitude of both sets of coefficients in the two cases of $\mu = [1, 0.1]$. The effect of this on the decay in magnitude of the produced impulse responses is seen in Figure 4.2c in which the magnitude of the impulse response is plotted. The decay rate after the length of filter order reduces as the step-size coefficient is increased. In Figure 4.2d the mean converged error is lower, especially in the cases $\mu = [0.1, 1]$. In these two cases the error is reduced with a similar rate after some iterations and makes a 'first convergence' where the error fluctuates around a similar level as the other cases of $\mu = [1 \times 10^{-2}, 1 \times 10^{-3}, 1 \times 10^{-4}]$. After this 'first convergence' the error then decreases further to reach true convergence. This result presents a question, if a more optimal solution is found with larger coefficient values then why is this not the solution found in every case? This could imply that the solution space for the undermodelled case is non convex. This would mean that the global minimum for the modelled or overmodelled case becomes a local minimum in the undermodelled case.

In the estimation of HRTF, shown in Figure 4.6d there is not an apparent 'first convergence'. Although, the two cases $\mu = [0.1, 1]$ do also achieve a lower converged error value than the other three cases of $\mu = [1 \times 10^{-2}, 1 \times 10^{-3}, 1 \times 10^{-4}]$. For the estimation of HRTF it is more difficult to make the same conclusion. This is due to the fact that in the magnitude response of the target filter, shown in Figure 3.3, there is a flat response in the lower frequencies.

Using pole-zero analysis can help explain some phenomena seen in filter design. The magnitude response of a given filter is a product of vectors on the z-plane. At a given frequency, which corresponds to a point on the unit circle, each pole and zero point has a vector to that frequency point. The magnitude response is then equal to the product of zero vector magnitudes divided by the product of pole vector magnitudes. Meaning that when the product of zero vector magnitudes are larger and the product of pole vector magnitudes are smaller this creates peaks. This happens when pole points are closer to the frequency point on the unit circle than the zero points. In high-order systems this becomes complicated to predict a magnitude response by observation of pole-zero plots. However, in simple cases, steep curves in magnitude response are created around frequencies where there is a large change in this fraction of vector magnitudes. Another effect of pole position is the impulse response decay, having poles closer to the unit circle will result in a

longer decay at that frequency. A pole directly on the unit circle will have no decay and outside of the unit circle will produce growth in signal amplitude at its nearest frequency.[11, Ch. 10]

It is often observed in filter design, that reducing the filter order results in a reduced frequency resolution, this is a result of having fewer pole and zero points which can create sharp changes in magnitude response. In adaptive filters, undermodelling a system therefore results in reduced accuracy when attempting to capture features with sharp transitions.

It is similarly observed that reduced filter orders produce a shorter decay of the response. This is a result of larger order systems often having poles closer to the unit circle. It is a result of design requirement, rather than a direct result of filter order itself.

Because of the selected filter order for each respective target IR, the headphone compensation filter and HRTF, the errors in estimation are different and not necessarily comparable. The order in the headphone compensation filter was reduced by a factor of roughly 40 and the order of the HRTF was reduce by a factor of roughly 10. This will be investigated further in the following section.

It is worth noting here that the input signal, a white Gaussian noise function, was generated with $-20\,\mathrm{dB}$ power level. This was due to initial testing with the direct form filter which did not converge with the selected step-size factor of $\mu = 0.03$. Adjusting the power level of the input signal can be seen as an additional scaling factor that acts upon the the target filter output and the estimated filter output and therefore also scales the output error calculated in the algorithms. Looking at both algorithms implemented Algorithm 2.4 and Algorithm 2.6, the coefficients are updated by multiplying output error, the step-size factor and the internal filter states which represent the gradient of the filter coefficients relative to the error.

Considering the results seen for selecting a larger step-size coefficient and remembering that the filter coefficients must update sufficiently slowly to maintain a valid solution, there are two possible outcomes:

1. The input signal with a power level of $-20\,\mathrm{dB}$ is too limiting and more optimal solutions are possible if using a higher power signal.

2. The limit on rate of change of filter coefficients is fixed and using a larger power level input signal will only results in a requirement of a smaller step-size factor to maintain validity.

In the case of the direct form filter which did not converge for the largest step-size factor it would suggest that the second outcome is most likely. However, in the case of the lattice form filter which can enforce stability through limiting the values of coefficients it would be interesting to investigate what the upper limit of the signal power and step-size coefficient combination is.

5.3 Minimum Order Investigation

This section contains the discussion on the results of the minimum order investigations. Here the effect of implementing an undermodelled adaptive IIR filter when estimating a known system was investigated.

When approaching this filter estimation task with a known impulse response as the target, an interesting benchmark is found by simply cutting the FIR impulse response. This is similar to estimating the system with an undermodelled optimal Wiener filter or adaptive filter with a vanishing step-size. Comparing the resulting magnitude spectra, and calculating the deviation from the full IR reveal the effect of reducing filter order. It is seen in Figures 4.17, 4.18, 4.9 and 4.10 that reducing the filter length worsens the filter resolution, that is the possible $\mathrm{dB\,Hz^{-1}}$ rate of change in magnitude response curve is reduced.

When visualising the magnitude spectra by plotting onto a logarithmic frequency axis, the impression is that man sharp peaks exist in the high frequencies. However, as the frequency density is orders of magnitude higher in this region, the $\mathrm{dB\,Hz^{-1}}$ may actually be comparable to relatively smooth curves in the low frequency range. Where the impulse response is cut from $M = 256$ to a FIR filter of order $M = 20$ in Figure 4.17b, the response has deviations from the full response of around 1 dB across the whole frequency range. Comparing this to the headphone compensation filter, similarly cut to $M = 460$ in Figure 4.9b, the deviations are much larger in the lower frequencies where there is a sharp roll-off below 25 Hz. In this case, the low frequency features demand a certain frequency resolution, and resulting filter order, to be resolved accurately.

Comparing the behaviour of the reduced order FIR filter to the solutions found for the undermodelled adaptive IIR filters gives insight into the benefit of using system identification with these chosen algorithms.

In Figure 4.23 the estimation of the HRIR with an IIR filter is compared directly with the cut FIR filters. For the case of $M = 20$ in Figure 4.23b the deviation shows there is little difference between the IIR and FIR filter magnitude spectra. In other cases such as order $M = 4$ there is much greater improvement made by implementing an IIR filter. Cases of order $M = [50100]$ in Figure 4.23d also show improvements in accuracy of the estimation, though to a lesser extent. An interesting result is comparing the cases of $M = 20$ and $M = 50$ where the case of $M = 50$ does not recover the flat low frequency response below the small peak at 500 Hz. In the high frequencies the larger $M = 50$ filter does improve upon the $M = 20$ resolution. This shows that in the case of the HRIR estimation a larger filter order can negatively impact the result in certain parts of the frequency response.

In Figure 4.16 the estimation of the headphone compensation filter with an IIR filter is compared directly with the cut FIR filters. In all cases of filter order here the impact of the IIR over the cut FIR filter is visible, though not necessarily improvement over the entire frequency range. The deviation form target for the low order cases of $M = 20, 100$ in Figure 4.16a, the IIR filter gives a reduced deviation at 10 Hz but in the region 15 Hz and 50 Hz the deviation is larger. The

deviation can vary depending on where the flat curve produced by the filters is crossed by the fluctuating response of the target filter. The lower order $M = 20$ filter produced a better response than order $M = 100$ between 25 Hz and 100 Hz because of this, though the roll-off at 25 Hz is not present in either case. In the deviation of the high-order cases in Figure 4.16d, the deviation is closer to zero for both order lengths $M = [220, 1000]$. The most significant improvement see was seen in the order $M = 1000$ case with a much improved resolution of the low frequency roll-off at 25 Hz.

Looking at the decay of the Impulse response over the whole impulse response, helps build understanding of why a higher order IIR filter produces a better estimation. In the low order estimations that the IR in early region is easily modelled for both the HRIR in Figure 4.22c and the compensation filter in 4.14c. Looking at the magnitude of the impulse response on a logarithmic axis emphasises the small details later in the response where the amplitude of the IR is very small.

Figure 4.12d shows the magnitude of the impulse responses for estimations of the headphone compensation filter. In the target IR magnitude a repeating pattern in the decay is seen, along with a low decay rate after 800 samples. The shorter filter orders such as $M = 100, 220, 460$ result in a steeper decay rate and more frequent oscillation in amplitudes. In the case for $M = 1000$ the pattern is seen in the decay and the overall decay rate begin to represent the target IR. Looking more closely at the target decay rate, there is a peak just above 2000 samples which would require a filter at least as long to capture accurately. One conclusion that can be made is that a shorter filter order results in less energy in the feedback part of the filter.

The magnitude of impulse response for the HRIR estimations in Figure 4.20 also show how increasing filter order also increases the energy in the late part of the decay. However the increase in this energy is not seemingly linearly related to the filter order selected. The increase in energy between $M = 50$ and $M = 70$ is much larger than that seen between $M = 70$ and $M = 100$. This suggests that for this filter the improvements between $M = [70, 100]$ lie in the better estimation of the region between 70 and 100 samples.

The very high filter order case shown in 4.15 explores filter orders required to achieve highly accurate modelling of the headphone compensation filter. In this result the filters all converged, although the challenge of solving such a large filter in the $M = 2300$ case was evident in the 4.15e where the error began diverging up to 1×10^5 iterations, upon convergence the error residual was significantly higher than the other cases. The interesting result is in the magnitude of the impulse response in Figure 4.15d around the peak seen above 2000 samples. The filter orders of $M = [2000, 2300]$ do capture this feature, however the errors of the longer filter generate noise in the impulse response. This noise in the result creates a larger degree of deviation from the target magnitude response as seen in Figure 4.15b, especially in the sharp peaks below 10 kHz.

It is important for a HRTF that the filter modelling is balanced for both channels of the HRTF, otherwise the result of any processing using these filters might not truly represent the measured HRTF. The results in Figures 4.24d and 4.25d showed

that the impulse response of the ipsilateral channel proved more difficult for the reduced order IIR filter to estimate because of multiple separate decay regions. The contralateral channel was comparatively well modelled by the larger $M = 150$ adaptive filter and this is confirmed by the deviation of the result from the target magnitude response in 4.24b. Checking the error convergence in Figure 4.24e and 4.25e showed that the ipsilateral channel estimation converged on a higher error residual manifold and therefore was not possible to accurately model the ipsilateral channel. As was seen in previous examples in the minimum order investigation, it was possible to achieve a reduced maximum deviation of the ipsilateral channel using a lower order filter of $M = 50$, seen in Figure 4.25b. This however gave a trade-off of reduced accuracy in the rest of the magnitude spectrum and in the estimation of the contralateral channel. This is an interesting result and suggests that with further optimisation of filter parameters, an adequate solution may be found for both channels, potentially in all combinations of azimuth, elevation and HATO orientation.

To attempt to find a minimum filter order requires a definition of an minimum error or deviation threshold, 1 dB can be arbitrarily chosen to make some comparison between the two systems studied here. For the headphone compensation filter estimation, the order reduction that achieved below 1 dB was $M = 1600$, more than a 60% reduction in filter order. For the contralateral channel HRTF estimation, the order reduction that achieved below 1 dB was $M = 50$, more than a 80% reduction in filter order. Finding a filter order that meets the 1 dB deviation criteria for both channels would require more fine tuned simulation of the binaural filter estimation.

5.3.1 Limitations and Future Work

It was identified in the step-size solution that more optimal filters may be found by using a larger step-size factor. This was linked to increased energy in the late decay region of the impulse response which could counter the effect of undermodelling. It could therefore be of interest to experiment with using higher power input signals in combination with stable algorithms to confirm if there is an upper bound on the step-size and input signal power relationship. As the error and deviation across magnitude response of the filter models are not linearly related to the filter length, a more detailed simulation of the error space for each case could identify the optimal minimum order for each system. This would also help to identify a filter order which balances the errors between binaural channel filter estimations.

Another option to more reliably find the true minimum error filter is to use algorithms which are less prone to convergence at local minima. In some cases this local convergence results in longer filters producing larger errors.

Finally further research could be completed in understanding of the solution space of the systems investigated here. One solution could include investigation of coefficient as a means of avoiding saddle points.[5]

6

Conclusion

It was found that lattice form filters do not produce more accurate filter estimations when compared to direct form filters and both are fully converged. The advantage of the stability test built in to lattice filters is confirmed in cases where the direct form filter did not converge. This was particularly advantageous in extremes of the solution space, such as implementing large step-size coefficients or solving very large filters. It was discovered that although stability can be guaranteed, this does not always result in finding the global minimum. In this case alternative algorithms which also ensure stability but are less sensitive to local minima, could be implemented.

Contrary to the theory, reducing the step-size coefficient resulted in an increased error residual and variance. It was proposed that this was due to the effect that the step-size coefficient has on the energy decay of the produced IIR filters, which resulted in marginal improvements in estimation in this late decay region. An additional factor to consider is the non-convexity of the solution space in undermodelled scenarios. Depending on the application, to could mean that larger step-sizes can sometimes lead to better performance.

It was confirmed that lower filter orders result in reduced frequency resolution, which limits the ability to model sharp transitions in the frequency response. This is particularly relevant for systems where low-frequency accuracy is critical.

IIR filters can increase this filter resolution compared to an FIR filter of equivalent order. In this study, the IIR filters produced were able to improve the filter resolution to an extent but were not able to drastically modify the resulting response. In some cases the estimated IIR filters made no improvements, or worsened the performance in specific frequency regions. In this regard it is important to use simulation in any new application in order to optimise the filter parameters.

A general recommendation for filter order requirement is not possible and requires simulation for each algorithm and target filter. An acceptable error residual or deviation must also be defined make such a claim. In cases where the target IR is a known system, investigation of the magnitude of the impulse response and the magnitude response are useful when made in consideration of the intended application. If the application hardware's frequency response doesn't reach the poorly modelled region of a low-order filter, there is no issue with undermodelling the system in such a way. For the headphone compensation filter estimation, the order reduction that achieved maximum deviation below 1 dB was $M = 1600$, more

than a 60% reduction in filter order. For the contralateral HRTF estimation, the order reduction that achieved maximum deviation below 1 dB was $M = 50$, more than a 80% reduction in filter order. The IIR filter of order $M = 50$ in the ipsilateral case did not meet this accuracy criteria, indicating further refinement is needed to balance filter performance across both channels. Alternatively, each channel may require it's own reduced order model to maintain accuracy.

Bibliography

[1] P. A. Regalia, *Adaptive IIR filtering in signal processing and control*. No. 90 in Electrical engineering and electronics, New York, NY [u.a.]: Dekker, 1. print. ed., 1995. Literaturangaben.

[2] C. Johnson, "Adaptive iir filtering: Current results and open issues," *IEEE Transactions on Information Theory*, vol. 30, no. 2, pp. 237–250, 1984.

[3] A. Antoniou and W.-S. Lu, *Practical Optimization: Algorithms and Engineering Applications*. Springer US, 2021.

[4] J. M. Giron-Sierra, *Digital Signal Processing with Matlab Examples, Volume 2*. Springer eBook Collection, Singapore: Springer, 2017.

[5] H. Fan and Y. Yang, "Analysis of a frequency-domain adaptive iir filter," *IEEE Transactions on Acoustics, Speech, and Signal Processing*, vol. 38, pp. 864–870, May 1990.

[6] M. L. Honig, *Adaptive filters*. No. 1 in The @Kluwer international series in engineering and computer science, Boston, Mass. [u.a.]: Kluwer Acad. Publ., 6. print ed., 1990.

[7] P. S. R. Diniz, *Adaptive filtering*. Cham: Springer, fifth edition ed., 2020.

[8] N. Agrawal, A. Kumar, V. Bajaj, and G. Singh, "Design of digital iir filter: A research survey," *Applied Acoustics*, vol. 172, p. 107669, Jan. 2021.

[9] G. Pepe, L. Gabrielli, S. Squartini, C. Tripodi, and N. Strozzi, "Deep optimization of parametric iir filters for audio equalization," *IEEE/ACM Transactions on Audio, Speech, and Language Processing*, vol. 30, pp. 1136–1149, 2022.

[10] T. J. Moir, *Rudiments of Signal Processing and Systems*. Springer International Publishing, 2022.

[11] A. V. Oppenheim, *Signals and systems*. Always learning, Harlow, Essex: Pearson Education, second edition, pearson new international edition ed., 2014.

[12] S. T. Alexander, *Adaptive Signal Processing*. Springer New York, 1986.

[13] M. H. Hayes, *Statistical digital signal processing and modeling*. New York, NY [u.a.]: Wiley, 1996. Literaturangaben.

[14] F. Brinkmann, "The fabian head-related transfer function data base," 2017.

[15] Y. Masuyama, G. Wichern, F. G. Germain, Z. Pan, S. Khurana, C. Hori, and J. L. Roux, "Niirf: Neural iir filter field for hrtf upsampling and personalization," 2024.

[16] Pitbub, "Hrtf azimuth," 2013. File: HRTFazimuth.png.

DEPARTMENT OF SOME SUBJECT OR TECHNOLOGY
CHALMERS UNIVERSITY OF TECHNOLOGY
Gothenburg, Sweden
www.chalmers.se

CHALMERS
UNIVERSITY OF TECHNOLOGY